Manipulating novel quantum phenomena using synthetic gauge fields

Manipulating novel quantum phenomena using synthetic gauge fields

Shao-Liang Zhang[1], Qi Zhou[2]
[1] *School of Physics, Huazhong University of Science and Technology, Wuhan 430074, P. R. China and*
[2] *Department of Physics and Astronomy, Purdue University, West Lafayette, IN, 47906*
(Dated: July 10, 2017)

The past a few years have seen fascinating progresses on creating and exploiting synthetic gauge fields for charge-neutral ultracold atoms. Whereas the synthesis of the gauge fields by itself is readily interesting, it is more exciting to explore the new era that will be brought by the interplay between synthetic gauge fields and many other degrees of freedom of the the highly tunable ultracold atoms. This Topic Review surveys recent developments of using synthetic gauge fields to manipulate novel quantum phenomena that are not easy to access in other systems. We will first summarize current experimental methods of creating synthetic gauge fields, including Raman scheme, shaken lattices, and Raman dressed lattices. We will then discuss how synthetic gauge fields bring new physics to non-interacting systems, including degenerate single-particle ground states, a quartic dispersion, topological band structures in lattices, and synthetic dimensions. As for interacting systems, we focus on novel quantum many-body states and quantum macroscopic phenomena induced by interactions in the presence of unconventional single-particle dispersions. For bosons, we discuss how a quartic dispersion leads to non-condensed bosonic states at low temperatures and at the ground state. For fermions, we discuss chiral superfluids in the presence of attractive s-wave interaction, where high partial-wave interactions are not required. We will eventually discuss the challenges in current experiments, and conclude with an outlook on what new exciting developments that synthetic gauge fields may bring us in the near future.

I. Introduction

Unlike electrons, electric and magnetic fields barely affect the orbital motions of charge-neutral atoms. Nevertheless, there had been long-term efforts to explore the possibility of creating synthetic gauge fields for atoms [1]. The hope was that the highly tunable atom-laser interaction might allow physicists to engineer effective Hamiltonians of atoms, which mimic those of electrons subject to gauge fields. The ultimate goal was even more ambitious. The synthetic gauge fields may not suffer the constraints on realistic electric and magnetic fields, such as the absence of magnetic monopoles. Moreover, a lot of degrees of freedom in atomic samples are highly controllable. Thus, the success of creating synthetic gauge fields was expected to bring physicists very rich quantum phenomena, many of which may not be easy to access in electronic systems.

In 2011, physicists eventually enjoyed the first realization of a synthetic gauge field for rubidium atoms. I. Spielman's group at NIST used a pair of Raman lasers to flip the hyperfine spin states of Rubidium atoms, and meanwhile transfer a moment to each atom[2–5]. Such spin-momentum locking allows the NIST group to engineer the single-particle dispersion of atoms, create synthetic electric and magnetic fields, and a one-dimensional synthetic spin-orbit coupling (SOC). A notable feature of these experiments is that they were performed in Bose-Einstein condensates (BECs) and thus opened the door for ultracold atom community to explore the interplay between synthetic gauge fields and macroscopic quantum phenomena.

Since NIST's experiments, many other groups in the world have also successfully realized and studied synthetic gauge fields for bosonic and fermionic atoms, in either the continuum or lattices. J. Zhang's group at Shanxi University[6] and M. Zwierlein's group at MIT[7] created one-dimensional synthetic spin-orbit couplings for nearly degenerate fermi gases. S. Chen's group at University of Science and Technology of China[8], P. Engels's group at Washington State University[9], Y. Chen's group at Purdue university[10], created synthetic SOC for bosons, and explored BECs subject to SOC either in a trap or in an optical lattice. I. Bloch's group at MPI [11] and W. Ketterle's group at MIT[12] applied Raman lasers to optical lattices, and realized the Harper-Hofstadter model. Alternatively, T. Esslinger's group at ETH[13], C. Chin's group at University of Chicago[14], and K. Sengstock's group at Hamburg University[15] used shaken lattices to produce synthetic gauge fields by the lattice potential itself without resorting to extra lasers. I. Spielman's group[16] and L. Fallani's group at University of Florence [17] used the hyperfine spin as a synthetic dimension to explore the edge currents. In addition to alkali atoms, B. Lev's group at Stanford University[18] and G. Jo's group at Hong Kong University of Science and Technology[19] realized synthetic SOC for dysprosium and ytterbium, respectively. J. Ye's group at NIST/JILA [20] and L. Fallani's group [21] realized SOC in an atomic clock lattice using ^{87}Sr and ^{173}Yb respectively. Whereas the studies in the literature has been mainly focusing on one-dimensional SOC for years, J. Zhang's group realized a controllable synthetic two-dimensional SOC for the first time in laboratories[22]. S. Chen's group also realized a Raman dressed lattice, where the effective Hamiltonian near certain points in the momentum space corresponds to a two-dimensional SOC [23]. Recently, B. Gadway's group

created a Raman dressed momentum-space lattice to observe the topological soliton state and to realize a quartic dispersion [24, 25].

Inspired by the aforementioned experimental progresses, the study of synthetic gauge fields has become one of the most important topics in ultracold atom physics. Enormous theoretical works have been published in the past a few years. As it is well known that gauge fields and SOC are crucial for the emergence of topological quantum matters in electronic systems, a major effort is to explore topological matters of ultracold atoms. Whereas there have been a number of review articles in the literature [26–29], this Topic Review will focus on aspects that have not been covered or systematically discussed before. In particular, we aim at discussing how synthetic gauge fields allow physicists to manipulating may allow physicists to access unconventional single-particle spectrum and interactions such that unconventional quantum phenomena, which are not easy to access in electronic systems, naturally arise.

We will start from a summary of the current experimental schemes of creating synthetic gauge fields, including Raman scheme, shaken lattices, and Raman dressed lattices in section II. The underlying mechanism of each method will be given and the connection between different schemes will be addressed. Section III focuses on unconventional dispersions induced by synthetic gauge fields in non-interacting systems. We will discuss how synthetic gauge fields allow physicists to create unconventional single-particle dispersions in both the continuum and lattices. Examples include a double-well structure in the momentum space, infinite degenerate single-particle ground states and a quartic dispersion. Non-interacting topological systems constructed by synthetic gauge fields will be introduced in section IV, such as topological band structures in lattices, non-Abelian Berry connections, and synthetic dimensions. In section V. we will discuss the interplay between synthetic gauge fields and interactions, and the resultant quantum many-body states and phenomena. In bosonic systems, we will address a fundamental question as to whether bosons may condense in the presence of synthetic SOC, which qualitatively changes the single-particle spectra at low energies. We will show that non-condensed bosonic states emerge when synthetic SOC significantly quenches the kinetic energy. As for fermions, we will discuss how synthetic SOC gives rise to synthetic high partial-wave interactions, and provides physicists a unique means to produce chiral superfluids, such as the $p_x + ip_y$ and $d_{x^2-y^2} + id_{xy}$, prototypical topological matters that are difficult to access in solid materials. In section VI, we will conclude with summarizing the current challenges in experiments, such as the heating effects and the probe of topological matters, and presenting our perspectives on possible future directions in the studies of synthetic gauge fields in ultracold atoms.

II. Current experimental schemes

1. Raman scheme

Alkali atoms have many different hyperfine spin states. For instance, rubidium atoms could be prepared at $F = 1$ states, which includes $|F = 1, m_F = \pm 1\rangle$ and $|F = 1, m_F = 0\rangle$. When the magnetic field is finite, the energy splitting includes the contribution from both the linear and quadratic Zeeman energies, which are denoted by Δ and ϵ, respectively. Applying a pair of Raman lasers with wavevectors k_1 and k_2, the difference in frequency is written as $\delta\omega = \omega_1 - \omega_2$. To simplify the notations, we assume that both k_1 and k_2 are along the x direction, though such alignment is not required in experiments. The Raman lasers induce the spin flip between $|1, 0\rangle$ and $1, \pm 1\rangle$, which is naturally accompanied by a momentum transfer $k_L = k_1 - k_2$. Thus, the single-particle Hamiltonian is written as

$$H = \begin{pmatrix} \frac{(k_x+k_L)^2}{2M} + \delta & \frac{\Omega}{2} & \\ \frac{\Omega}{2} & \frac{k_x^2}{2M} - \epsilon & \frac{\Omega}{2} \\ & \frac{\Omega}{2} & \frac{(k_x-k_L)^2}{2M} - \delta \end{pmatrix}. \tag{1}$$

where k_x and M is the momentum and mass of atoms, $\delta = \Delta - \delta\omega$, Ω is the Raman coupling strength [3]. For convenience, $\hbar = 1$ has been set. A more rigorous derivation of Eq.(1) can be found from reference [26, 30].

In the regime where δ is large, we could focus on the lowest branch of the eigenstates of Eq.(1), which is well separated from the other two branches. Near the band bottom of the lowest branch, the Hamiltonian can be well approximated by

$$H_{\text{eff}} = \frac{(k_x - A_x)^2}{2M}, \tag{2}$$

where the vector potential A_x depends on k_L, δ and Ω[3]. By further introducing a time- or spatially-dependent A_x, synthetic electric and magnetic fields can be created in experiments[4, 5]. In the regime $\delta \approx \epsilon$, where the quadratic Zeeman energy compensates the linear one, $|1, 0\rangle$ and $|1, -1\rangle$ become nearly degenerate. Eq.(1) can be simplified as

$$H_{\text{SOC}}^{\text{1D}} = \frac{1}{2M}\left(k_x - \frac{k_L}{2}\sigma_z\right)^2 + \frac{\Omega}{2}\sigma_x - \frac{h}{2}\sigma_z, \tag{3}$$

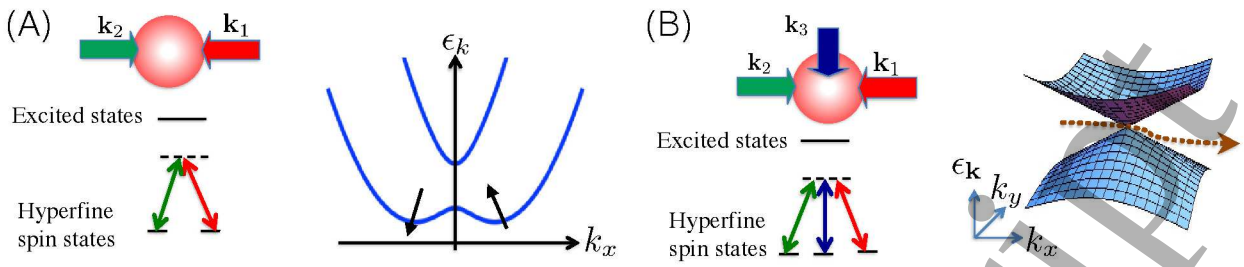

FIG. 1: Raman scheme produced SOC. (A) Two counter-propagating lasers (red and green arrows) are applied to an atomic cloud (red sphere). Far-detuned transition between the hyperfine spin states and excited states leads to the Raman coupling between two hyperfine spin states. The single-particle dispersions of these two hyperfine spin states are shifted to the opposite directions in the momentum space. A finite gap opens at $k = 0$ for any finite Raman coupling strength. The single-particle dispersion has two minima, at which the spins (black arrows) are not completely orthogonal. (B) Three lasers (red, green, and blue arrows) are applied to an atomic cloud. Each laser dresses one and only one hyperfine spin state. The resultant single-particle dispersion contains a single Dirac point in the $k_x - k_y$ plane. This Dirac point is stable against adjustments of microscopic parameters in the system, and could be moved around in the momentum space (curved brown arrow).

where σ_x and σ_z are the spin-1/2 Pauli matrices, and $h = \delta - \epsilon$. $k_x \to k_x + \frac{\delta_k}{2}$ has been used for simplicity. Eq. (3) is a Hamiltonian describing a one-dimensional SOC, and the time-reversal symmetry is broken in this Hamiltonian if Ω is finite. The single-particle ground state becomes doubly degenerate when $\delta = \epsilon$, as shown in Fig.(1A).

Since the original NIST experiment in 2011, most experimental studies have been focusing on Eq.(1,2,3). A two-dimensional SOC eluded experiments for years. In 2015, J. Zhang's group realized for the first time in laboratories a two-dimensional SOC using three hyperfine spin states of potassium-40, $|1\rangle = |9/2, 3/2\rangle$, $|2\rangle = |9/2, 1/2\rangle$ and $|3\rangle = |7/2, 1/2\rangle$[22]. Three lasers are applied in experiments, and the frequencies of the lasers and the magnetic field are chosen such that each laser dresses one and only one of these three hyperfine spin states, as shown in Fig (1B). The Hamiltonian for this three level system is written as

$$H_{\rm SO}^{\rm 2D} = \sum_{i=1}^{3} \left(\frac{(\mathbf{k} - \hbar \mathbf{k}_i)^2}{2M} + \delta_i \right) |i\rangle\langle i| - \sum_{i' \neq i} \frac{\Omega_{ii'}}{2} |i\rangle\langle i'|, \tag{4}$$

where $\mathbf{k}$ denotes the mass and momentum of atoms respectively, $\mathbf{k}_i$ are the wave vectors of the three lasers, δ_i are the energy detuning and $\Omega_{ii'}$ are the Rabi frequency of the effective two-photon process. Three cyclically coupled states were original proposed in the ring scheme for a symmetric arrangement of lasers[31]. Related schemes have also been theoretically studied [32–34]. In fact, arbitrary laser configurations work for three cyclically coupled states, provided that $\mathbf{k}_1 - \mathbf{k}_2$ and $\mathbf{k}_2 - \mathbf{k}_3$ are not parallel to each other. In particular, under this condition, the Hamiltonian in Eq.(4) always supports a Dirac point in the momentum space, regardless of the microscopic parameters. Define the plane spanned by the two vectors $\mathbf{k}_1 - \mathbf{k}_2$ and $\mathbf{k}_2 - \mathbf{k}_3$ as the $x - y$ plane, the position of the Dirac point, $\mathbf{p}_0$, is determined by

$$\begin{aligned} -\frac{(\mathbf{k}_1 - \mathbf{k}_2) \cdot \mathbf{p}_0}{M} + \delta_1 - \delta_2 &= -\frac{\Omega_{12}\Omega_{13}}{2\Omega_{23}} + \frac{\Omega_{12}\Omega_{23}}{2\Omega_{13}} \\ -\frac{(\mathbf{k}_2 - \mathbf{k}_3) \cdot \mathbf{p}_0}{M} + \delta_2 - \delta_3 &= -\frac{\Omega_{12}\Omega_{23}}{2\Omega_{13}} + \frac{\Omega_{13}\Omega_{23}}{2\Omega_{12}}. \end{aligned} \tag{5}$$

Near $\mathbf{p}_0$, the energy spectrum becomes linear along both the k_x and k_y directions, and the Hamiltonian is written as

$$H_{\rm SO}^{\rm 2D} = (\lambda_{x1} p_x + \lambda_{y1} p_y)\sigma_x + (\lambda_{x2} p_x + \lambda_{y2} p_y)\sigma_y, \tag{6}$$

where $p_{i=x,y}$ has been redefined as $p_i - p_{0,i}$ for simplicity. By a proper rotation of the momentum and the spin, the Hamiltonian is written as

$$H_{\rm SO}^{\rm 2D} = \lambda_x p'_x \sigma'_x + \lambda_y p'_y \sigma'_z \tag{7}$$

where both λ_x and λ_y are well tunable in experiments. A highly controllable two-dimensional SOC is thus realized.

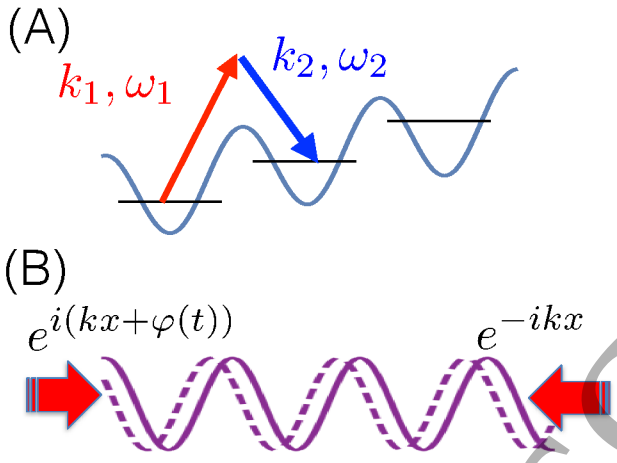

FIG. 2: (A) Raman dressed lattice. Two lasers(red and blue vectors) provide atoms photo-assistant tunneling to overcome the energy mismatch induced by a linear field gradient. This tunneling naturally carries a position-dependent phase imprinted by the Raman lasers such that a synthetic magnetic field can be created in an optical lattice. (B) Shaken lattice. When the two counter-propagating lasers have a time-dependent relative phase, the interference pattern is no longer static. The atoms thus feel a time-dependent lattice potential. When the relative phase is time-periodic, the lattice potential also becomes time-periodic and gives rise to Bloch-Floquet bands, which can used to design either unconventional single-particle dispersions or topological band structures.

2. Raman dressed lattice

In addition to the continuum, Raman lasers could be applied to optical lattices. Using a magnetic field gradient, which produces an energy mismatch between the nearest neighbor sites, the bare tunneling in the lattice is suppressed, as shown in Fig (2A). Adding Raman lasers to the lattice, the Raman transition helps atoms to overcome the energy mismatch through the laser-assisted tunneling, which naturally carries a phase determined by the lasers[35–37]. Such complex tunneling is written as $t \sim e^{-i\delta\mathbf{k}\cdot\mathbf{R_m}}$, where $\delta\mathbf{k}$ is the momentum transferred in the Raman process and $\mathbf{R_m}$ is the real space coordinate of the lattice site $\mathbf{m}$. Bloch's group has applied this scheme to a two-dimensional square lattice[11]. The field gradient is applied to the x direction only, and the tunneling along the y direction is not affected. The photon-assisted tunneling along the x direction becomes $t_x \sim e^{-i\frac{\pi}{2}(m+n)}$, where the lattice coordinate is given by $\mathbf{R_m} = (m, n)$. Thus, the synthetic magnetic flux per plaque is $\pi/2$. A similar design was implemented by Ketterle's group[12]. If two different hyperfine spin states, which have opposite magnetic momenta, are uploaded to the lattice, the field gradient has different signs for them. As a result, the synthetic magnetic fields are opposite. This provides physicists a simple realization of quantum spin Hall effect. The Raman scheme can also be extended to a titled double-well optical lattice, in which the energy mismatch between the left and right wells in the same lattice site is naturally provided by the lattice itself and an external field is not required. The resultant synthetic magnetic flux becomes staggered[38]. Recently, Ketterle's group has extended the Raman scheme to a titled double well lattice, in which the s and p orbitals serve as a pseudospin [39, 40]. Whereas in the single particle level, the Hamiltonian is equivalent to SOC in the continuum, the advantage in this scheme is that, the inter-spin interaction, which is represented by the inter-orbital interaction, can be much weaker than the intra-spin (intra-orbital) interaction, because of the spatial separation of the s and p orbitals. In this scheme, it is much easier to realize the so-called stripe phase, in which both the minima of the doubly degenerate single-particle states are occupied[30, 41, 42].

3. Shaken lattices

An alternative scheme to engineer the tunneling in an optical lattice is to shake it. Here, we take a one-dimensional optical lattice as an example. The interference of two counter propagating lasers e^{ikx} and e^{-kx} gives rise to a periodic potential $\sim \cos^2(kx)$. Adding a time-dependent phase difference $2\varphi(t)$ between these two lasers provides one a time-dependent potential $\sim \cos^2(kx + \varphi(t))$, where $k = \frac{\pi}{d}$ and d is the lattice spacing, as shown in Fig (2B). Choosing $\varphi(t) = kf\cos(\omega t)$, the Hamiltonian in the framework of Floquet theory is written as

$$H_S - i\hbar\partial_t = \frac{p^2}{2M} + V\cos\left[\frac{2\pi}{d}(x + f\cos(\omega t)\right] - i\hbar\partial_t. \tag{8}$$

The time dependence of the lattice potential can be eliminated by a gauge transformation $x' = x + f\cos(\omega t)$, $t' = t$,

$$H_{\rm S} - i\hbar\partial_{t'} = \frac{(p' - A(t'))^2}{2M} + V\cos\left(\frac{2\pi x'}{d}\right) - i\hbar\partial_{t'} \tag{9}$$

where $A(t) = fM\omega\sin(\omega t)$ is a time-dependent gauge potential. Thus, shaking a lattice is equivalent to Raman dressed lattice, in the sense that both could produce complex laser assisted tunneling. The technique advantage of the shaken lattice is that external lasers are not required.

One could further apply a transformation $x' = x + f\cos(\omega t)$, $p' = M\dot{x}'$, and the Hamiltonian becomes

$$H'_{\rm S} = \frac{p'^2}{2M} + V_0\cos\left(\frac{2\pi x'}{d}\right) + M\omega^2 f x'\cos(\omega t), \tag{10}$$

which describes a lattice subject to a time-dependent electric field. Eqs.(8,9,10) are all equivalent. One can choose any of them to analyze the shaken lattices.

Shaken lattices were first studied by E. Arimondo's group at University of Pisa[43]. It was discovered that shaking allows one to suppress the tunneling amplitude and change the sign of the tunneling in the s band. C. Chin's group at University of Chicago considered a larger shaken frequency such that the shaking strongly hybridize the s and p bands[14]. Consequently, a double-well structure shows up in the momentum space, and the single-particle ground state becomes two-fold degenerate. Besides modifying the single-particle dispersion, shaking an optical lattice also allows experimentalists to engineer topological band structures in both one and two dimensions. T. Esslinger's group used a shaken honeycomb lattice to realize the topological Haldane model for the first time in experiments[13]. K. Sengstock's group realized Ising-XY spin models by shaking an triangular optical lattice[15].

III. Unconventional single-particle dispersions

In the previous section, we have surveyed the currently available experimental techniques to realize synthetic SOC in laboratories. Here, in Section III, we will theoretically analyze how synthetic SOC may lead to unconventional single-particle dispersions. Some single-particle physics, including the double-well potential in the momentum space, the topological band structures, and the Wilson lines, has been experimentally explored. The quartic dispersion was recently studied experimentally using the momentum space lattice. Nonsymmorphic symmetries have not been studied experimentally in ultracold atoms so far.

1. Double-well structure in the momentum space

For the Raman scheme in the continuum, it is rather clear that a double-well structure naturally emerges in the single-particle spectrum, since the Raman lasers shift the spin-up and spin-down atoms towards opposite directions in the momentum space. Similar single-particle spectrum also shows up in a shaken lattice [14]. Consider Eq.(8), Floquet theorem could be applied to study the quasi-energy in this time-periodic system. A time-periodic one-dimensional lattice, $V(x,t) = V\cos^2\left[k_0 x + \frac{f}{2}\cos(\omega t)\right]$, can be expanded as

$$V(x,t) = \sum_n \tilde{V}_n(x,t) = \sum_n V_n(x)e^{in\omega t}, \tag{11}$$

where V_n is the amplitude of a given Fourier component [44, 45]. The explicit expressions of V_n are given by

$$V_n(x) = \begin{cases} \frac{i^n}{2}VJ_n(f)\cos(2k_0x) & n \in even, \\ \frac{i^{n+1}}{2}VJ_n(f)\sin(2k_0x) & n \in odd, \end{cases} \tag{12}$$

where $J_n(f)$ is the Bessel function of the first kind. Physically, $\tilde{V}_0$ represents a static lattice, and $\tilde{V}_n(x,t)$ can be viewed as a dynamically induced lattice potential that excites the system by a multiple-photon energy $n\hbar\omega$. In Floquet theorem, the solution of the time-periodic Schrödinger equation is written as $\Psi(x,t) = e^{-i\epsilon t}\Phi(x,t)$, where ϵ is the quasienergy and $\Phi(x, t + 2\pi/\omega) = \Phi(x,t)$. The Floquet mode can be written as $\Phi(x,t) = \sum_{mkn} c_{mkn}\phi_{mk}(x)e^{in\omega t}$, where $\phi_{mk}(r)$ are the eigenstates of the static lattice. The Floquet-matrix representation is obtained as

$$\sum_{m',n'} (\mathcal{V}^{m,m'}_{n-n',k} + (\epsilon^0_{m'k} + n'\hbar\omega)\delta_{n,n'}\delta_{m,m'})c_{m'k,n'} = \epsilon c_{mk,n}, \tag{13}$$

where $\mathcal{V}^{m,m'}_{n-n',k} = \int dx\phi^*_{mk}(x)V_{n-n'}(x)\phi_{m'k}(x)$. Eq.(13) tells one that side bands of the m-th band of the static lattice form by absorbing or emitting n photons. For instance, the s band can absorb one photon and becomes resonant with the p band, as shown in Fig (3A). Focusing on these two resonant bands, the Hamiltonian is written as

$$H_{\rm S} = [(t_s - t_p)\cos(k_x d) + \delta]\sigma_z - \Omega_1\sigma_x. \tag{14}$$

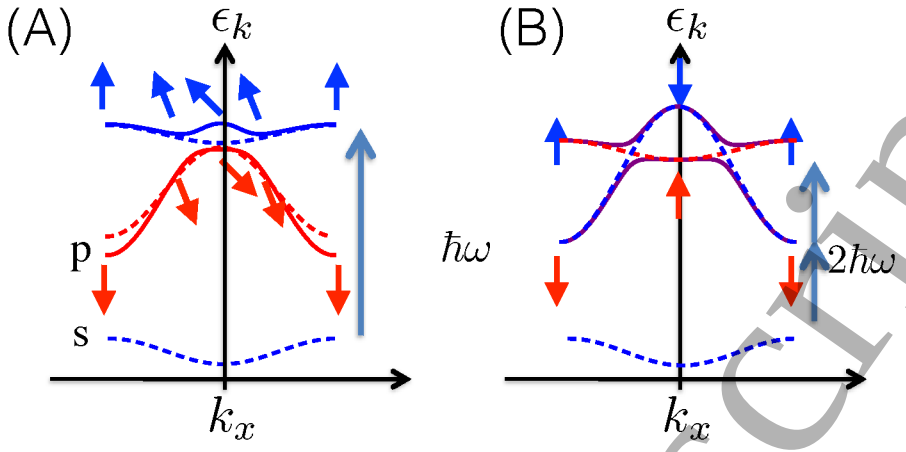

FIG. 3: (A) In a shaken lattice, the s band could absorb one photon energy $\hbar\omega$ and becomes degenerate or nearly degenerate with the p band. The band hybridization leads to a double-well structure in the momentum space. (B) When the s band needs to absorb two photons to be degenerate or nearly degenerate with the p band, the hybridized bands have finite Zak phases. When k changes for one reciprocal lattice vector, the pseudospin defined by the s and p bands rotates for 2π on the Bloch sphere.

where $d = \pi/k_0$ is the lattice spacing, δ is the one-photon detuning, and $\Omega_1 = \frac{V}{2}J_1(f)\langle W_{s,R_i}|\sin(2k_0x)|W_{p,R_i}\rangle$, and W_{s,R_i} and W_{p,R_i} are the Wannier wave functions of the s and p bands located at site R_i, respectively. Eq.(14) exactly corresponds to a SOC, in which bands in an lattice serve as a pseudospin [45]. The above discussions can be directly generalized to two dimensions. It has been shown that, in a two-dimensional shaken square lattice, the single-particle dispersion has four degenerate minima [46, 47].

2. Infinitely degenerate single-particle ground state

If the spin-momentum locking exists along more than one direction, the single-particle ground states may become highly nontrivial. For a two-dimensional isotropic SOC, the Hamiltonian is written as

$$H_{\rm iso}^{\rm 2D} = \frac{1}{2M}(\mathbf{k}^2 + 2\lambda\mathbf{k}\cdot\boldsymbol{\sigma}_\perp), \tag{15}$$

where $\mathbf{k} = (k_x, k_y)$ and $\boldsymbol{\sigma}_\perp = (\sigma_x, \sigma_y)$. For any finite value of λ, the minimum of the kinetic energy is a circle with the radius $|\mathbf{k}| = \lambda$ in the momentum space. Thus the single-particle grounds state become infinitely degenerate. Similarly, one could consider a three-dimensional isotropic spin-orbit coupling, and the Hamiltonian is written as

$$H_{\rm iso}^{\rm 3D} = \frac{1}{2M}(\mathbf{k}^2 + 2\lambda\mathbf{k}\cdot\boldsymbol{\sigma}). \tag{16}$$

where $\mathbf{k} = (k_x, k_y, k_z)$ and $\boldsymbol{\sigma} = (\sigma_x, \sigma_y, \sigma_z)$. The single-particle minimum now becomes a sphere. For both cases, a fundamental question naturally arises, what are the ground states of interacting systems, as any infinitesimal interaction becomes non-perturbative?

Whereas we will address the interaction effects in section V, here we would like to highlight another unique phenomena arising from these infinitely degenerate single-particle ground states. Density of States at low energies, which is denoted by $\mathcal{N}(\epsilon)$, is a crucial quantity to determine the properties of a many-body system at low temperatures. For ordinary quadratic dispersions, textbook results tell one that $\mathcal{N}(\epsilon)$ scales as ϵ^α, and $\alpha = 1/2$, 0, and $-1/2$ in 3D, 2D, and 1D, respectively. Applying isotropic spin-orbit couplings, it has been shown that $\mathcal{N}(\epsilon)$ can be significantly enhanced[48–50]. For instance, in 2D, for a 2D isotropic SOC as shown in Eq.(15) , $\alpha = -1/2$, similar to an ordinary 1D system. In 3D, the same SOC leads to a constant $\mathcal{N}(\epsilon)$ at low energies, i.e., $\alpha = 0$. Alternatively, a 3D isotropic SOC in Eq.(16) gives rise to an exponent $\alpha = -1/2$. For all cases, it is clear that $\mathcal{N}(\epsilon)$ has been significantly enhanced compared with the conventional systems. This can be regarded as an effective dimension reduction.

The enhanced $\mathcal{N}(\epsilon)$ has a significant impact on many-body physics even in the absence of interaction. For ordinary bosonic systems, though the condensate transition temperature T_{BEC} is finite in 3D, a condensate only forms at zero temperature in 2D. In 1D, there is no condensate even at the ground state. Such significant difference entirely comes

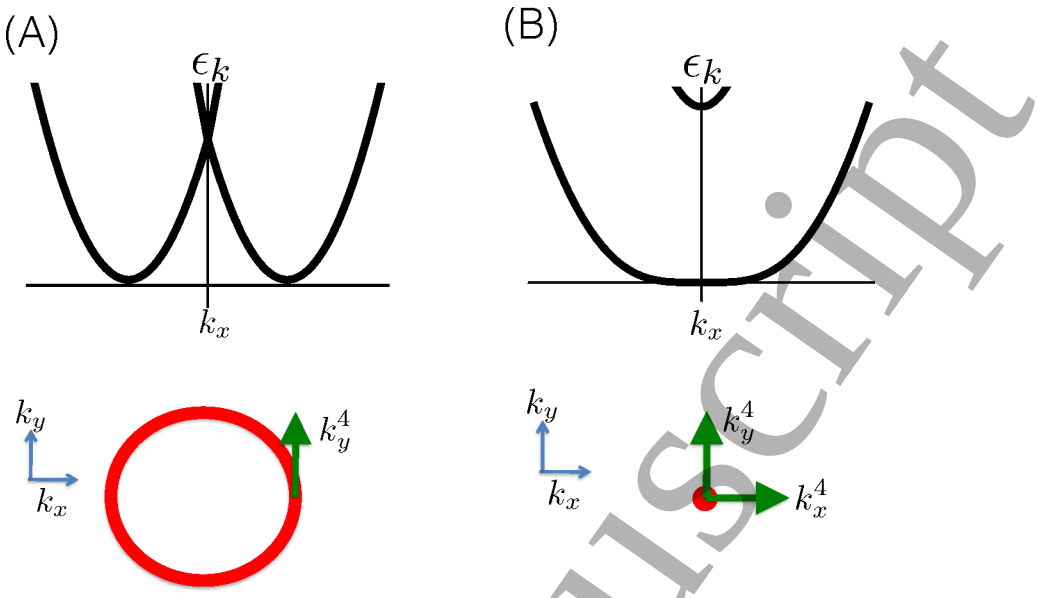

FIG. 4: (A) When the Raman coupling strength Ω is zero in Eq.(3) and Eq.(18) is zero, the two branches of single-particle dispersion intersect at the origin. For the 2D Hamiltonian in Eq. (18), the single-particle energy minima form a circle in the momentum space (red circle). (B) When the Raman coupling strength Ω reaches a critical value Ω_c, the circle shrinks to one point. Near this point, the single-particle dispersion is quartic. Such quartic dispersions are much flatter than conventional quadratic dispersions and significantly enhance fluctuations and correlations in the system.

from the distinct $\mathcal{N}(\epsilon)$ at low energies. It can also be understood from the general Mermin-Wagner theorem that the continuous $U(1)$ symmetry cannot be spontaneously broken in $D = 1$ at the ground state [51]. In the presence of an isotropic SOC in 3D, as $\mathcal{N}(\epsilon)$ has been enhanced to $\epsilon^{-1/2}$, condensate does not exist even at the ground state. For the 2D isotropic SOC, it suppresses T_{BEC} down to zero, as the low-energy $\mathcal{N}(\epsilon)$ is similar to that of an ordinary 2D system. Alternatively, in 2D, a 2D isotropic SOC is sufficient to suppress the condensation even at zero temperature. Introducing interaction to the system, the question on the fate of a condensate becomes even more intriguing. We will discuss the interaction effect in section V.

3. Quartic dispersions

In conventional systems, the kinetic energy is often quadratic near the minimum, ie., $\epsilon \sim k^2$. Now let us consider Eq.(3) when $h = 0$. When $\Omega = 0$, the two single-particle branches intersect at $k = 0$, and the spectrum has two degenerate minima, which are located at finite momenta $\pm k^*$ where $k^* = k_L/2$, as shown in Fig (4A). In the Raman scheme, the theoretical limit $\Omega = 0$ corresponds to the absence of SOC coupling, and the dispersion of different spin or pseudospin components are independent. Nevertheless, the limit of a vanishing Ω may be achieved in other schemes, where the term $\Omega\sigma_x$(or $\Omega\sigma_z$) is simply a Zeeman energy. Turning on a finite but small Ω, a gap opens at $k = 0$. there are two degenerate minima with a finite k^* for all experimental setups. With increasing Ω, the value of k^* decreases, and eventually, only one minimum exits at $k = 0$ when Ω is large enough. At the critical point $\Omega_c = k_L^2/(2M)$, the two minima just merge into a single one. If one expands the kinetic energy near $k = 0$, one obtains,

$$E(k) = -\frac{k_L^2}{8M} + \frac{k^4}{2Mk_L^2} + \mathcal{O}(k^6). \tag{17}$$

One sees that the single-particle dispersion becomes quartic, as shown in Fig.(4B). [52, 53]. Similar to the Raman scheme, a shaken lattice could also produces a quartic dispersion, since the double well structure there is also tunable. By changing either the shaken amplitude or frequency, the two minima in the band structure may also merge into a single one, and thus a quartic dispersion arises [46, 47].

The above discussions can be straightforwardly generalized to two dimensions[46]. Consider a Hamiltonian,

$$H_{\mathrm{R}}^{2D} = \frac{1}{2M}\Big\{k_x^2 + k_y^2 - 2\lambda\big(k_x\sigma_x + k_y\sigma_y\big) + 2\lambda\Omega\sigma_z\Big\}. \tag{18}$$

When $\Omega = 0$, the above equation reduces to Eq.(15), and the single-particle ground state is a circle, as discussed before. Turning on Ω, the radius of the circle decreases. When $\Omega = \Omega_c^0 \equiv \lambda$, the circle shrinks to a single point. At this critical point, the kinetic energy at small k can be expanded as

$$\epsilon_{\mathbf{k}} = \frac{1}{2M}\Big\{ -2\lambda^2 + \frac{1}{4\lambda^2}\big(k_x^2 + k_y^2\big)^2 + \mathcal{O}(k^6)\Big\}. \tag{19}$$

It is clear that the single-particle dispersion becomes quartic in both the k_x and k_y directions. Though the single-particle ground state now becomes unique, such quartic dispersion significantly enhances $\mathcal{N}(\epsilon)$ at low energies. In particular, in 2D, $\mathcal{N}(\epsilon) \sim \epsilon^{-1/2}$.

Similar discussions can be applied to a 2D shaken lattice. Shaking the lattice along both directions symmetrically, i.e., with the same frequency and amplitude, there may exist four minimum of the kinetic energy. Tuning the shaken amplitude or frequency, the four minima may merge into a single minimum[46, 47]. At this critical point, the kinetic energy is written as

$$E(k) = \big(k_x^4 + k_y^4\big) + \mathcal{O}(k^6). \tag{20}$$

Compare it with Eq. (19), the rotation symmetry in the momentum space reduces to a four-fold one. This is not surprising, since the underlying square lattice has a four-fold symmetry. If the shaking is anisotropic, i.e., the shaking frequencies or amplitudes are different along the x and the y directions, only two minima exist. When these two minima merge into a single one, a quartic dispersion shows up along one direction in the momentum space, and the other direction retains the quadratic dispersion.

IV. Topological band structures

1. Topological band structures

Besides controlling the shape of single-particle dispersions, synthetic gauge fields also allow one to engineer topological band structures. Consider a one-dimensional shaken lattice, in section III.1, we discussed the parameter regime $\omega \approx E_g$, i.e., one-photon resonance. Here, we consider two-photon resonance $\omega \approx E_g/2$, i.e., the $s(p)$ band adsorbs (emits) two photons to become resonant with the $p(s)$ band, as shown in Fig. (3B). Now the dynamically generated lattice that is relevant for providing the inter-band hybridization is $V_2(x) = -VJ_2(f)\cos(2k_0x)/2$. As $V_2(x)$ has even parity, it cannot couple the s and p orbitals in the same lattice site, and the leading inter-orbital tunneling occurs between the nearest neighbor sites. The Hamiltonian in the momentum space is thus written as

$$H'_{\mathrm{S}} = \big[(t_s - t_p)\cos(k_x d) + \delta\big]\sigma_z - 2\Omega_2 \sin(k_x d)\sigma_x. \tag{21}$$

where $\Omega_2 = \frac{V}{2}J_2(f)\langle W_{s,\mathbf{R}_i}|\cos(2k_0x)|W_{p_x,\mathbf{R}_i+d\hat{x}}\rangle$ [44, 45]. Compare with Eq.(14) in section III.1, we note that that the off-diagonal term now also depends on the momentum. Moreover, we have treated s and p band as a pseudospin-1/2. As k increases from $-\pi/d$ to π/d, this pseudospin-1/2 rotates on the Bloch sphere. The winding number then determines the Zak phase, which is the Berry phase in crystals with periodic band structures [54]. It is easy to find out that, when $\delta < |t_s - t_p|$, the Zak phase is written as

$$\varphi_{\mathrm{Zak}} = i\int_{-\pi/d}^{\pi/d} \langle u_k(x)|\partial_k|u_k(x)\rangle dk = \pm\pi \tag{22}$$

The plus and minus signs correspond to the two different bands of Hamiltonian (21). When $\delta > |t_s - t_p|$, the Zak phase vanishes, and the bands become topologically trivial.

Whereas the 1D shaken lattice provides one a simple and illuminating example of engineering topological band structures, it is even more interesting to consider 2D systems. Here, we use a checkerboard lattice as an example[55]. As shown in Fig. (5A), the Hamiltonian of a circularly shaken checkerboard lattice is written as

$$H_{\mathrm{S}}^{\mathrm{2D}} - i\hbar\partial_t = \frac{\hat{\mathbf{P}}^2}{2M} + V(x + f\cos\omega t, y + f\sin\omega t) - i\hbar\partial_t, \tag{23}$$

where f and ω are the shaken amplitude and frequency respectively, $\mathbf{r} = (x, y)$ and $V(\mathbf{r}) = -V_0\left(\cos^2(\frac{\pi x}{d}) + \cos^2(\frac{\pi y}{d}) + 2\zeta\cos(\frac{\pi x}{d})\cos(\frac{\pi y}{d})\right)$ is the lattice potential, ζ is a tunable constant. By a simple transformation $x \to x + f\cos\omega t, y \to y + f\sin\omega t, t \to t$, one sees that equation (23) is equivalent to

$$H_{\mathrm{S}}^{\mathrm{2D}} - i\hbar\partial_t = \frac{(\hat{\mathbf{P}} - \mathbf{A}(t))^2}{2M} + V(\mathbf{r}) - i\hbar\partial_t, \tag{24}$$

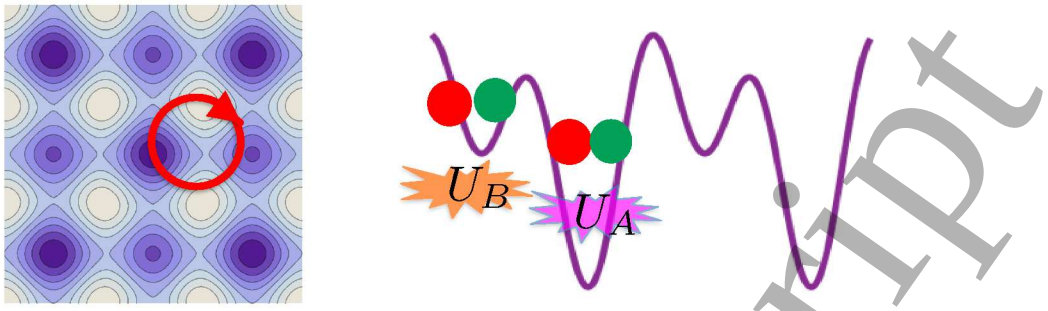

FIG. 5: A contour plot of the lattice potential of a checkerboard lattice. When circularly shaking such lattice, Chern bands arise. The pseudospin defined by the A and B sublattices gives rise to a pseudospin-orbit coupling near the center of BZ. Two component fermions (red and green spheres) have onsite attractive interactions U_A and U_B in the lattice. The interplay between the attractive interaction and the circular shaking produces a chiral d-wave superfluid.

which describes a static lattice subject to a circularly polarized time-periodic gauge field $\mathbf{A}(t) = (A\sin\omega t, -A\cos\omega t)$, and $A = fM\omega$, except for a trivial position independent constant. This type of Hamiltonian also apply for solids subject to external periodic drivings [56].

The checkerboard lattices can be easily created for ultracold atoms [57, 58]. A finite ζ produces an energy offset Δ between A and B sublattice sites, and suppresses the inter-sublattice tunneling. However, once such a lattice is periodically driven, the $\mathbf{A}(t)\cdot\hat{\mathbf{P}}$ term provides atoms a photo-assisted tunnelling to overcome this energy mismatch. The Hamiltonian in the rotating wave approximation is written as

$$K_{\rm S}^{\rm 2D} = \begin{pmatrix} \epsilon_{A\mathbf{k}} & \Omega_{\mathbf{k}}e^{i\varphi_{\mathbf{k}}} \\ \Omega_{\mathbf{k}}e^{-i\varphi_{\mathbf{k}}} & \epsilon_{B\mathbf{k}} \end{pmatrix}, \tag{25}$$

where $\epsilon_{A\mathbf{k}} = 4t_A\cos k_x d\cos k_y d + 2t'_A(\cos 2k_x d + \cos 2k_y d) - \delta$, $\epsilon_{B\mathbf{k}} = 4t_B\cos k_x d\cos k_y d + 2t'_B(\cos 2k_x d + \cos 2k_y d)$, $\Omega_{\mathbf{k}}e^{i\varphi_{\mathbf{k}}} = 2\Omega(i\sin k_x d - \sin k_y d)e^{-ik_x d}$ and $\varphi_{\mathbf{k}} = \arg\{(i\sin k_x d - \sin k_y d)e^{-ik_x d}\}$. t_A (t_B) and t'_A (t'_B) characterize the nearest- and next-nearest neighbor tunnelings in the A(B) sublattice, Ω is the amplitude of the photon-assisted inter-sublattice tunneling, and $\delta = \Delta - \hbar\omega$ is the detuning. Near the center of Brillouin Zone, the off-diagonal term can be approximated by $e^{i\varphi_{\mathbf{k}}} \sim k_x\eta_x + k_y\eta_y$. Thus, it can be considered as Rashba type of pseudospin-orbit coupling where the sublattice index represents the pseudospin $\boldsymbol{\eta}$.

Using Eq. (25), the Berry connection $\mathcal{A}_n(\mathbf{k}) = i\langle u_n(\mathbf{k})|\partial_{\mathbf{k}}|u_n(\mathbf{k})\rangle$ and Berry curvature $\Omega_n(\mathbf{k}) = \nabla\times\mathcal{A}_n(\mathbf{k})$ can be evaluated, where n is band index of the eigenstates, and $|u_n(\mathbf{k})\rangle$ is the corresponding periodic Bloch wave function. The Chern number is obtained from $C = \int_{\rm BZ}\Omega_n(\mathbf{k})d\mathbf{k}$. In the strong hybridization limit of $4(t'_A - t'_B) - 4|t_A - t_B| < \delta < 4(t'_A - t'_B) + 4|t_A - t_B|$, the Chern numbers of the two bands are $C = 1$ and $C = -1$, respectively. This scheme to produce a Chern band is general. One could use a bipartite lattice with A and B sublattice sites, which can be treated as a pseudospin-1/2 [55]. Tuning the tunnelings between A and B sublattice sites allows one to engineer the effective pseudospin-orbit coupling. In fact, the underlying mechanism of the ETH experiment to create the topological Haldane model is similar[13]. Circularly shaking a honeycomb lattice, which consists of two sublattices, a complex tunneling between two sites in the same sublattice was created to open up the gap at the Dirac point of the honeycomb lattice, and Chern bands form.

2. Non-abelian Berry connection, Wilson line, and nonsymmorphic symmetries

Whereas the current experimental efforts have been mainly focusing on studying the abelian Berry curvature [59], a pioneering experiment was recently done by I. Bloch's group to explore the non-abelian Berry connection and Wilson line [60]. A strong force was applied to an atomic cloud uploaded to a honeycomb lattice. In this strong force limit, the lowest two bands of the honeycomb lattice becomes effectively degenerate, and the population of atoms could be redistributed between these two bands in quantum dynamical evolutions. Thus, the abelian Berry curvature is no longer capable to capture the topological properties of the system. Under this force, the momentum changes from $\mathbf{k}_i$ to $\mathbf{k}_f$, and the quantum dynamics is governed by the Non-abelian Berry connections [61],

$$\mathbf{A}_{mn}(\mathbf{k}) = i\langle u_{m\mathbf{k}}(\mathbf{r})|\nabla_{\mathbf{k}}|u_{n\mathbf{k}}(\mathbf{r})\rangle. \tag{26}$$

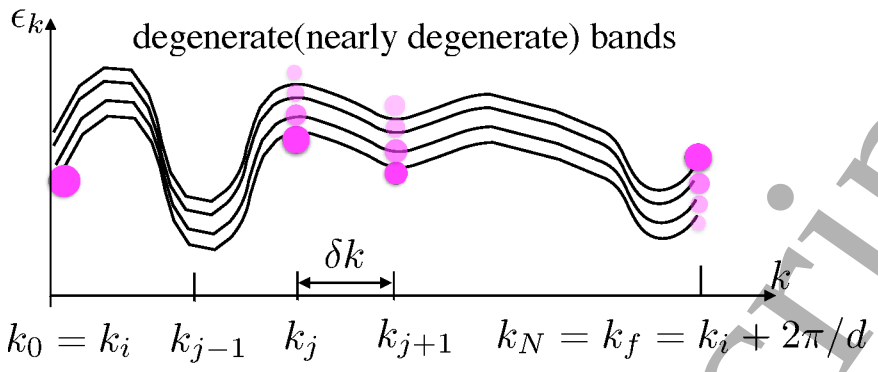

FIG. 6: Black curves represent degenerate or nearly degenerate bands. For clarity, they have been shifted along the horizontal direction. A particle (pink sphere) initially stays at k_i in a given band. Applying a strong force F, where Fd is much larger than the splitting of the nearly degenerate bands, the particle has finite probability to occupy other bands when its momentum changes. Dividing such dynamics into N ($N \to \infty$)steps, when k_j changes to k_{j+1} in a single step, the redistribution of the weight of the wavefunction in each band is determined by the non-abelian Berry connections. For a finite momentum change from $k_0 = k_i$ to $k_N = k_f$, the distribution of the weight of the wavefunction is determined by Wilson line. The sizes of spheres indicate the weight of the wavefunction in each band.

The Wilson line, as the line integral of the non-abelian Berry connection, tells one the probability of a particle, which initially starts from the n-th band, $|n\mathbf{k}\rangle$, in the degenerate manifold, to occupy the m-th band, $|m\mathbf{k}\rangle$, at the final momentum $\mathbf{k}_f$. The matrix representation of the Wilson line is written as $W_{mn} = \langle m\mathbf{k}_f|\prod_j \hat{W}_j|n\mathbf{k}_i\rangle$, where $\hat{W}_j = e^{id\mathbf{k}\cdot\hat{\mathbf{A}}_j}$, $\hat{\mathbf{A}}_j = \sum_{mn}\mathbf{A}_{mn}(\mathbf{k})|m\mathbf{k}_{j+1}\rangle\langle n\mathbf{k}_j|$, determines an infinitesimal evolution when we divide the trajectory from $\mathbf{k}_i$ to $\mathbf{k}_f$ into many infinitesimal steps, as shown in Fig.(6). Using this method, Wilson line was reconstructed for the first time in laboratories.

In this experiment, the Wilson line is determined by the structure factor of the honeycomb lattice, $(e^{i\mathbf{G}\cdot\mathbf{r}_A}, e^{i\mathbf{G}\cdot\mathbf{r}_B})$, where $\mathbf{r}_A$ and $\mathbf{r}_B$ are the positions of the A and B sublattices in a unit cell of a honeycomb lattice, and $\mathbf{G}$ is a reciprocal lattice vector. The non-abelian Berry connection and Wilson line could exist in a much broader ultracold atom systems. In particular, when nonsymmorphic symmetry is respected by the lattice structure, band touching points exist in the lattice structure[62–64], The non-abelian Berry connection and Wilson line are naturally required to characterize the topological properties of the system. In the following discussions, we will use a simple 1D model

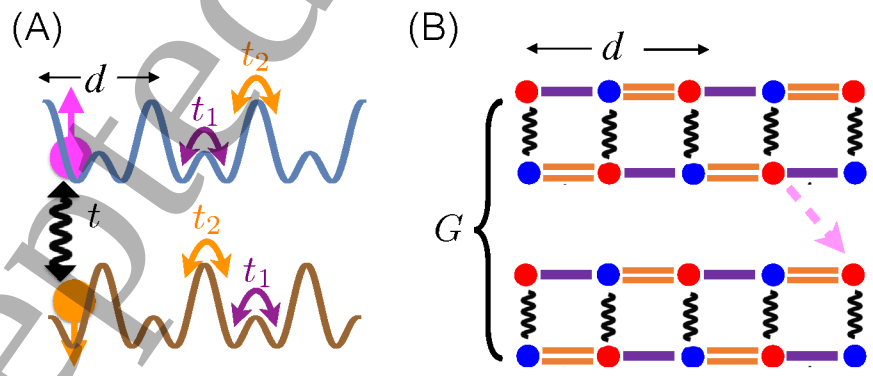

FIG. 7: (A) Each double well lattice is characterised by two tunnelling amplitudes, t_1 and t_2. The inter-leg tunnelling is denoted by t. (B) Tight-binding model and glide inversion symmetry. Red and blue dots represent the left and right well in each lattice site. t_1, t_2, and t are represented by single, double, and curved lines. After the glide inversion, a red well shifted to a red well on the other leg, as indicated by the pink arrow.

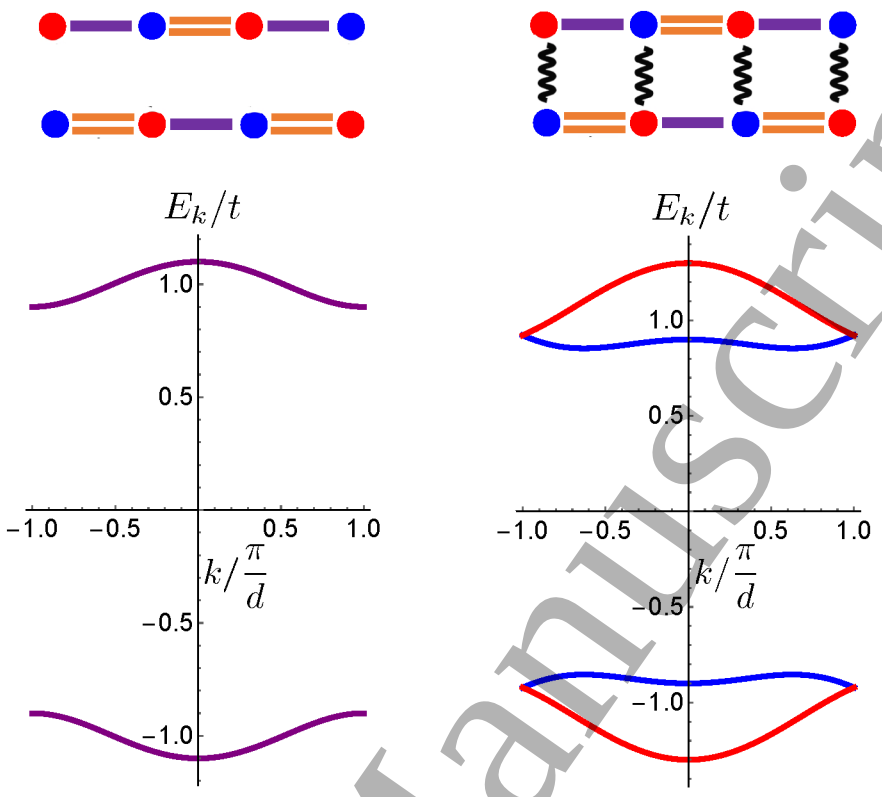

FIG. 8: Typical energy spectrum of the two-leg SSH chain. When the inter-leg tunnelling is zero, each band has a double degeneracy. When the inter-leg tunnelling is turned on, band crossings still exist in BZ due to the glide inversion symmetry.

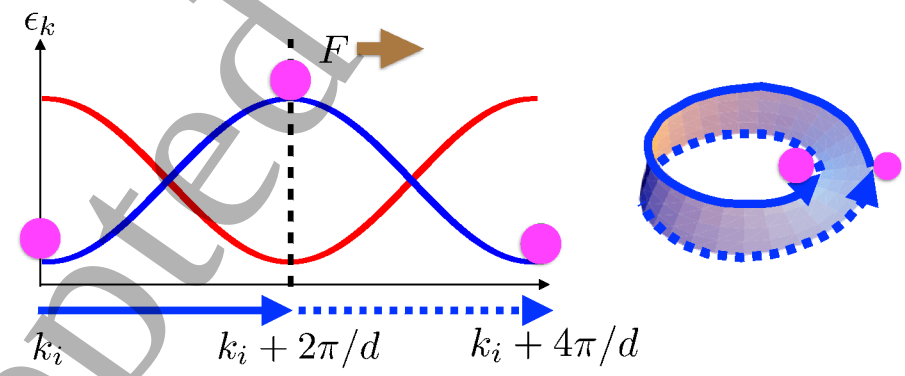

FIG. 9: The eigenvalues of the glide operation on the red and blue bands are $+e^{ikd/2}$ and $-e^{ikd/2}$, respectively. They intersect once when k changes by $2\pi/d$ such that the ground (the first excited) band becomes the first excited (ground band) across the BZ boundary. Under a force F (brown arrow), an atom (pink sphere), which initially stays at the ground band, moves in the momentum space. When k changes by $2\pi/d$, it arrives at the top of the first excited band. When k changes by another $2\pi/d$, it becomes back to the original place in the ground band. This mimics the Mobius strip, in which an object ends up at the other side of the strip when finishing one circle.

to illuminate the non-abelian Berry connection, Wilson line, and nonsymmorphic symmetry [65].

Consider two chains of double-well lattices, each of which is shifted from the other by half of the lattice spacing, as shown in Fig.(7). These two chains are coupled to each other by the inter-chain tunneling t. For each double-well lattice, it is described by the well established two-leg Su-Schrieffer-Heeger model, which includes two tunneling amplitudes t_1 and t_2. In the absence of the inter-chain tunneling, these two double-well lattices represent two topologically distinct configurations of the Su-Schrieffer-Heeger model. Apparently, in a finite system, if one double-well lattice has edge states, the other must not. Now consider a finite t, it is clear that the glide symmetry, one of the nonsymmorphic symmetries, exists in this system. This can be seen from the fact that the Hamiltonian remains unchanged under the glide operation, a combination of the mirror reflection in the synthetic direction, which corresponds to the flip of the two hyperfine spins, and a shift along the physical direction for half of the lattice spacing. There is an alternative scheme to realize an equivalent model [66].

A notable result of the glide symmetry is that, band crossings must exist in BZ, as shown in Fig (8). As two glide operations correspond to a translation for one lattice spacing, the eigenvalue of G^2 must be e^{ikd}. Therefore, the eigenvalues of G are $\pm e^{ikd/2}$. When k changes by 2π, the plus and minus sign in front of the eigenvalues must switch with each other. Thus, there must exist band crossings between two bands in BZ. Due to these symmetry protected band crossings, non-abelian Berry connections and Wilson lines are required to to describe the topological properties of the system. In particular, applying a force, an atom, which is initially at the lowest band, will end up at the top of the first excited band, when k changes by $2\pi/d$, a reciprocal lattice vector, as shown in Fig (9). Only when k changes by $4\pi/d$, the atom could come back to the same momentum at the original band This mimics a Mobius strip. Such nonsymmorphic symmetry could also be studied in 2D[67]. A two-dimensional lattice with nonsymmorphic symmetry has been recently realized in experiments[23].

3. Synthetic dimension

There is an alternative way to view synthetic SOC. If one treats the hyperfine spin states as the lattice sites in a synthetic dimension, one readily obtains a $D+1$ dimensional system in a physical D-dimensional systems [68]. For instance, a 1D atomic gas with multiple hyperfine spin states subject to SOC gives one a 2D system, which is discrete in the synthetic dimension. In particular, the tunnelings in the synthetic dimension is dependent on the spatial coordinates in the physical dimension. This is not surprising, as the spin flip depends on momentum. This is can be easily seen from the Raman coupling term, which is proportional to $\Omega e^{ik_L x}\sigma^+ + h.c.$. This corresponds to a magnetic field in such 2D system, as the phase accumulate by a particle finishing a closed loop in this 2D plane is finite and depends on k_L. Using this method, edge states on synthetic Hall ribbons have been observed [69, 70]. A unique advantage of synthetic dimension is that the boundary conditions in this dimension can be engineered for realizing a space with nontrivial topology, such as cylinder, torus, and Möbius strip [68, 71].

V. Interaction effects

1. Bosons: Condensed or not?

When there are degenerate single-particle ground states, a fundamental question naturally arises, where do bosons condense to? This question has been studied extensively in the literature[72–75]. The general understanding is that, the so called fragment condensates are not stable. This is mainly due to two reasons. First, it may cost additional Hartree-Fock energies if bosons occupy more than one state in the degenerate manifold [72]. Second, in reality, a small perturbation may destroy the fragment condensate and turn it to an ordinary condensate[75]. Introducing synthetic gauge field, not only that single-particle dispersions may exhibit degenerate single-particle ground states, but also novel effective interactions may be induced by the synthetic gauge fields in the degenerate manifold.

1a. 1D SOC

Consider the double-well dispersion in the Raman scheme as shown in Fig. 1(a). In this case, $h=\delta-\epsilon=0$ and the ground state of single particle Hamiltonian (3) has Z_2 symmetry, as the Hamiltonian remains unchanged under the transformation $k_x\to -k_x$ and $\sigma_z\to-\sigma_z$. We define the left and right well as a pseudospin-1/2, and the interaction is rewritten as

$$U_{\rm int}=g_1\hat{n}_\uparrow^2(\mathbf{r})+g_2\hat{n}_\downarrow^2(\mathbf{r})+g_{12}\hat{n}_\uparrow(\mathbf{r})\hat{n}_\downarrow(\mathbf{r}), \tag{27}$$

where $g_1(g_2)$ and g_{12} are the intra- and inter-pseudospin interactions, respectively. For simplicity, we assume $g=g_1=g_2$ here. It is worth mentioning that g and g_{12} here are different from the bare intra- and inter-hyperfine spin interaction. As shown in Fig. (1A), when the Raman coupling strength Ω is finite, the spins at the bottoms of both the left and the right wells are superpositions of the bare hyperfine spin states. Thus, g and g_{12} are modified by a

finite Ω. Extensive studies have explored how g/g_{12} determines the ground state [30, 41, 42, 76, 77]. When $g > 2g_{12}$, the ground state is a so called stripe phase

$$|S\rangle = (\frac{a^\dagger_{k_0} + a^\dagger_{-k_0}}{\sqrt{2}})^N|0\rangle, \tag{28}$$

where $a^\dagger_{-k_0}$ ($a^\dagger_{k_0}$) is the creation operator for bosons at the bottom of the left(right) well. The interference of the two plane waves e^{ik_0x} and e^{-ik_0x} creates a density wave in the real space. There also exists a spin density wave, due to the non-orthogonal hyperfine spins at the bottoms of the left and the right wells, as explained before. When $g < 2g_{12}$, the ground state is a so called plane-well phase,

$$|P\rangle = a^{\dagger N}_{-k_0}|0\rangle, \text{ or, } |P\rangle = a^{\dagger N}_{k_0}|0\rangle. \tag{29}$$

The ground state spontaneously breaks the Z_2 symmetry, and the condensation and magnetization occur simultaneously at zero temperature.

In experiments, though it is difficult to tune the bare hyperfine spin interaction of Rb atoms, g/g_{12} is controlled by changing the Raman coupling strength Ω, which determines the orientations of the hyperfine spins at the bottoms of the dispersion. It was found out that the transition from the stripe phase to the plane-wave phase occur at a finite Ω at zero temperature. This critical value decreases as temperature increases, as the plane-wave phase has larger entropy than the stripe phase at finite temperatures[78, 79]. Theoretical studies have also shown that, at even larger inter-pseudospin interactions, a magnetic phase could also occur in the normal state when the temperature is above the condensate transition temperature [80, 81].

Whereas a double-well structure in the single-particle dispersion can also be produced in a shaken lattice (see section III.1), the interaction effects are completely different. As shown in Fig. (3B), the orientations of the pseudospin at the bottoms of the left and right wells are parallel to each other in the shaken lattice. Thus the effective interaction is ferromagnetic. At zero temperature, the ground state is a plane-wave phase. At finite temperatures, the right- and left-moving domains have been observed in experiments [14].

1b. 2D SOC

For 2D isotropic SOC in Eq.(15), which gives rise to a circle as the minimum of the kinetic energy, the problem becomes even more interesting, as the single-particle degeneracy becomes infinity. To solve this challenging question, a few different approaches have been used in the literature. Mean-field schemes based on trial wave functions of condensates found out that the ground state is either a plane-wave phase or a stripe phase[42]. However, this approach does not answer the the fundamental question as to whether and how bosons may condense on this infinitely degenerate circle. To search for possible exotic states, few-body problems have been studied [50]. To gain insights, we start from a two-body problem, in which the bosons are confined in this circle. Project the interaction in Eq. (27) to the basis of single-particle eigenstates, we obtain the effective interaction in the subspace composed of the infinitely degenerate single-particle ground states is written as the effective interaction can be formulated as

$$U_{\text{eff}} = \sum_{\phi_1,\phi_2,\phi_3,\phi_4} U^{\phi_3,\phi_4}_{\phi_1,\phi_2} \hat{L}^\dagger_{\phi_1} \hat{L}^\dagger_{\phi_2} \hat{L}_{\phi_3} \hat{L}_{\phi_4}/4, \tag{30}$$

where

$$U^{\phi_3,\phi_4}_{\phi_1,\phi_2} = g_{12}e^{i(\phi_1-\phi_4)} + g_2 + g_1 e^{i(\phi_1+\phi_2-\phi_3-\phi_4)}, \tag{31}$$

$\hat{L}^\dagger_\phi$ ($\hat{L}_\phi$) is the creation (annihilation) operator on the circle $\mathcal{L}$ composed by all single-particle ground states, and ϕ is the polar angle.

A notable feature in Eq.(31) is that the effective interaction depends on the angles $\phi_{i=1,2,3,4}$ as analogous to the synthetic high partial wave scatterings induced by SOC in 3D [82]. As a result of such angular dependence, regardless of the ratio of the inter- and intra-spin interaction, the ground state is written as

$$|SF\rangle = \frac{1}{\sqrt{\pi}} \int_0^\pi d\phi e^{2i\nu\phi} L^\dagger_\phi L^\dagger_{\phi+\pi}|0\rangle, \tag{32}$$

where ν is an integer different from 0 and 1. Thus there is an infinite degeneracy at the ground states. The above wavefunction describes a small Schrödinger-Cat. In particular, the ground state energy is exactly zero, despite that we

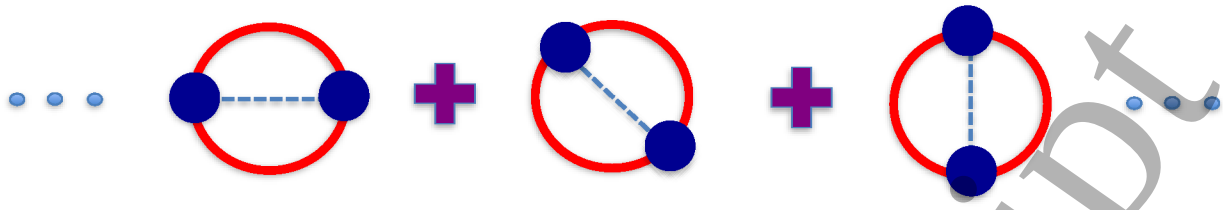

FIG. 10: The ground state of two interacting bosons on the circle of single-particle energy minima. These two bosons prefer to occupy the two opposite points on the circle to minimize the Hartree-Fock energy. Meanwhile, the infinite degeneracy allows these two bosons to be scattered to any other pair of opposite points on the circle. The energy gained by such scatterings cancel the Hartree-Fock energy such that the ground state energy is zero.

consider repulsive interaction here. An alternative approach based on T-matrix also found out that the renormalized interaction on the circle becomes zero, when the momentum of the two scattering particles are antiparallel to each other[83, 84]. This result is consistent with the exact solution of a two-body problem here.

There are mainly two reasons for the state in Eq.(32) to become the ground state. First, the angular dependence significantly modifies the Hartree-Fock energy. On the circle, the Fock states can be written as either $|\phi,\theta\rangle = \hat{L}^\dagger_\phi \hat{L}^\dagger_{\phi+\theta}|0\rangle$ for $\theta \neq 0$ or $|\phi,0\rangle = \hat{L}^\dagger_\phi \hat{L}^\dagger_\phi|0\rangle/\sqrt{2}$. θ is the relative angle between the two bosons on the circle. A straightforward calculation shows that, when $g_{12}/(g_1+g_2) > 1$, states with $\theta = \pi$ minimize the Hartree-Fock energy. Thus, two bosons prefer to occupy two opposite points on the circle, i.e., fragmentation occurs. This is a significant consequence of SOC. Without SOC, it is well-known that it is difficult for a fragmentation to occur in homogenous systems, because of the cost of Fock energy when bosons occupy different momentum states [72]. Second, a state $|\phi,\pi\rangle$ can be scattered to another state $|\phi',\pi\rangle$ with arbitrary ϕ'. This mimics the scatterings of pairs of fermions near the Fermi surface in superconductors or superfluids. Such off-diagonal couplings reduces the interaction energy, and the ground state becomes a superposition of all states $|\phi,\pi\rangle$, as shown in Fig (10). Interestingly, the energy reduction from the off-diagonal coupling exactly cancels the Hartree-Fock energy. Thus, the ground state is exactly zero.

The two-body problem can be generalized to an arbitrary N-body problem. A cluster of bosons, which consists of a few atoms, have been found to form correlated states, instead of simple condensates[85]. Here, we would like to emphasis an intrinsic difference in the thermodynamic limit. For small N, the ground state is either a (small) Schrödinger-Cat state or a plane-wave phase. When N is large, it requires multiple steps of scattering to couple one fragmented condensate $|F\rangle_\phi = \hat{L}^{\dagger N/2}_\phi \hat{L}^{\dagger N/2}_{\phi+\pi}|0\rangle$ to another one $|F\rangle_{\phi'}$, since the interaction can scatter only two atoms from $(\phi,\phi+\pi)$ to another pair of angles $(\phi',\phi'+\pi)$. The effective coupling between these two states is then exponentially small. The energy gained by the superposition of all fragmented states quickly decreases with increasing N. In the thermodynamic limit, the phase transition point recovers the mean-field result. Another important ingredient is the anisotropy of the SOC. When SOC is anisotropic, i.e., has different strengths along different directions, the single-particle ground state is no longer a circle, but contains only two minima, similar to a 1D SOC. The Schrödinger-Cat states are no longer stable, and the problem reduces to the one considered in the previous section. Thus, the ground state is either a plane-wave or a stripe phase. Besides the aforementioned approaches, feminization has also been used. Based on the observation that the single-particle Density of States becomes a 1D like one $\sim \epsilon^{-1/2}$, it was argued that the many-body ground state of bosons should be feminized in the dilute limit, similar to ordinary 1D systems [86–88]. The questions regarding the connections between the feminization and the few-body results remain open so far. Besides the studies of SOC in the continuum, trapped BECs have also been investigated. An interesting phenomena is that the trapping potential gives rise to half-quantum vortex state [89–91].

1c. Condensate depletion

In non-interacting systems, we have seen that the enhanced $\mathcal{N}(\epsilon)$ is crucial in determining whether a condensate may exist a variety of SOC. Taking into account interaction effects, the $\mathcal{N}(\epsilon)$ of non-interacting systems may not be relevant any longer for the stability of a BEC. The reason is that, when the single-particle dispersion has an infinite degeneracy, the interaction effect is in general highly non-perturbative and an infinitesimal interaction may force bosons to condense in the thermodynamic limit. The plane-wave phases and stripe phase are such examples, as explained in the previous section. Consequently, one needs to analyze Density of States of low-energy excitations, i.e., the Bogoliubov quasiparticles, to determine whether a condensate is stable.

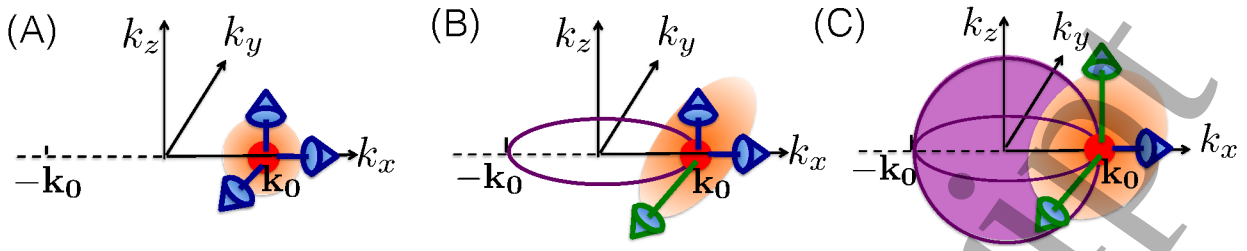

FIG. 11: From left to right, condensate depletions in case (a, b, c). In the absence of soft modes in case (a), the quasiparticle spectrum is linear (blue arrows) along all directions. The depletion (orange cloud) is the same as that in an ordinary system. Thus a BEC (red sphere) is stable. In case (b), the single-particle energy minima is a circle (purple circle), and one soft mode (green arrow) emerges. Both quantum and thermal depletions are enhanced. In case (c), the single-particle energy minima becomes a sphere (purple sphere). Two soft modes show up, and a BEC is not stable at any finite temperatures.

Here, we use a plane wave phase in 3D as an example to demonstrate how different types of SOC give rise to distinct condensate depletions. We consider a general SOC in 3D,

$$H^{3\mathrm{D}} = \frac{1}{2M}\left(\mathbf{k}^2 + 2\sum_{\alpha}\lambda_\alpha k_\alpha \sigma_\alpha\right), \tag{33}$$

where $\alpha = x, y, z$ and λ_α characterizes the strength of SOC in different directions. A few particular SOC are illuminating examples, (a) $\lambda_x \neq 0$, $\lambda_y = \lambda_z = 0$, (b) $\lambda_x = \lambda_y, \lambda_z = 0$, (c) $\lambda_x = \lambda_y = \lambda_z, g_1 = g_2 = g_{12}$. (a) is the case when SOC exists along only one direction, (b) is the Rashba coupling, and (c) is referred to as isotropic SOC and interaction. In case (a), bosons condense at one of the kinetic energy minima, $k_x = \lambda_x$. We then gradually turn on SOC along the y and the z direction to realize case (b) and (c). For these three cases, the Bogoliubov quasiparticle spectrum $E_{\mathbf{q}}$ in the small momentum limit have distinct expressions,

$$\begin{aligned}
&\text{(a):} \quad E_{\mathbf{q}} = \sqrt{\tfrac{\mu}{M}(q_x^2 + q_y^2 + q_z^2)} \\
&\text{(b):} \quad E_{\mathbf{q}} = \sqrt{\tfrac{\mu}{M}(q_x^2 + \tfrac{q_y^4}{4\lambda_x^2} + q_z^2)} \\
&\text{(c):} \quad E_{\mathbf{q}} = \sqrt{\tfrac{\mu}{M}\left(q_x^2 + \tfrac{(q_y^2+q_z^2)^2}{4\lambda_x^2}\right)},
\end{aligned} \tag{34}$$

where $q = |\mathbf{q}|$, and μ is the chemical potential. In case (a), the Bogoliubov quasiparticle spectrum is the same as that of an ordinary BEC. It is linear and isotropic along all three directions, $E_{\mathbf{q}} = cq$, where $c = \sqrt{\mu/M}$. In case (b), the Bogoliubov quasiparticle spectrum becomes quadratic along the q_y direction, i.e., $\sim cq_y^2/\lambda_x$ [76, 92–94]). This can be regarded as a soft mode, since the sound velocity vanishes along the q_y direction. The spectrum is still linear along the other two directions. In case (c), an additional quartic dispersion emerges along the q_z direction. This requires that both SOC and interaction are isotropic.

The quartic dispersions, or soft modes, in case (b) and (c) enhance Density of States of quasiparticles $\rho(\epsilon)$. For case (a), (b) and (c), it is straightforward to show that

$$\rho^{(a)}(\epsilon) \sim \epsilon^2, \quad \rho^{(a)}(\epsilon) \sim \epsilon^{3/2}, \quad \rho^{(c)}(\epsilon) \sim \epsilon. \tag{35}$$

We could compare the above results with the Density of States of quasiparticles in ordinary systems. In the absence of SOC, the phonon-like quasi-particle ($E_{\mathbf{q}} = cq$) leads to $\rho(\epsilon) \sim \epsilon^{D-1}$, where $D = 1, 2, 3$ is the dimension. Thus, $\rho^{(a)}(\epsilon)$, $\rho^{(b)}(\epsilon)$ and $\rho^{(c)}(\epsilon)$ correspond to effective dimensions $D_{\text{eff}} = 3, 5/2$ and 2 respectively. This effective dimension reduction is produced by SOC, which suppresses the kinetic energy along one or more directions. In particular, $D_{\text{eff}} = 5/2$ and 2 in case (b) and (c), respectively, indicate that condensate depletions are significantly enhanced in these two cases.

The quantum depletion in Bogoliubov theory can be estimated using $n_0^{ex} \approx \mu \int_0^\mu d\epsilon \rho(\epsilon)/(2\epsilon)$, since it is mainly determined by the excitation below the chemical potential. In case (a), the quantum depletion is the same as an ordinary condensate without SOC, since $\rho(\epsilon)$ remains unchanged after turning on such SOC. For case (b) and (c), the quantum depletions are enhanced by a factor of $(\kappa_x\xi)^{\frac{1}{2}}$ and $(\kappa_x\xi)$, respectively, where $\xi = (2M\mu/\hbar^2)^{-\frac{1}{2}}$ is the healing

length. The enhancement of quantum depletion is also studied numerically [93]. Similarly, the thermal depletion at low temperatures is written as $n_T^{ex} \approx \mu T \int_0^T d\epsilon \rho(\epsilon)/\epsilon^2$. Again, in case (a), $n_T^{ex}/n \sim (T/\mu)^2$ for $T < \mu$, similar to the result for ordinary systems without SOC. In case (b), $n_T^{ex}/n \sim (T/\mu)^{\frac{3}{2}}$, and the thermal depletion grows faster than case (a), as the quartic dispersion along the q_y direction allows more thermal fluctuations at low temperatures. Case (c) is the most interesting one. Since $\rho^{(c)}(\epsilon) \sim \epsilon$, it is straightforward to see that there is a logarithmic divergence in the thermal depletion, as $n_T^{ex} \sim \int d\epsilon/\epsilon$. Such a logarithmic divergence is a characteristic feature of an ordinary 2D system, and shows that a condensate is not stable at any finite temperature in case (c). The schematics of the condensate depletions in case (a-c) are shown in Fig.(11).

1d. Algebraic quantum liquid

In the previous section, we have seen that SOC significantly enhances both the quantum and thermal depletions. Nevertheless, the quantum depletion remains finite at zero temperature in all cases that have been considered so far. A natural question is then, whether SOC may completely destroy the condensate even at the ground state? An even deeper question is, what is the new ground state when a condensate is completely destroyed? As bosons naturally condense at zero temperature, it is known to be a long-standing challenge to create a non-condensed bosonic state at the ground state. Here, we discuss a simple scheme using synthetic SOC to suppress condensation. Once the condensate vanishes at the ground state, a variety of unconventional quantum phenomena emerge, including the rise of an algebraic quantum liquid and the deconfinement transition of topological excitations. Moreover, we will see that synthetic SOC provides one an atomic simulator of the quantum Lifshitz model, a fundamentally important model in condensed matter and high energy physics.

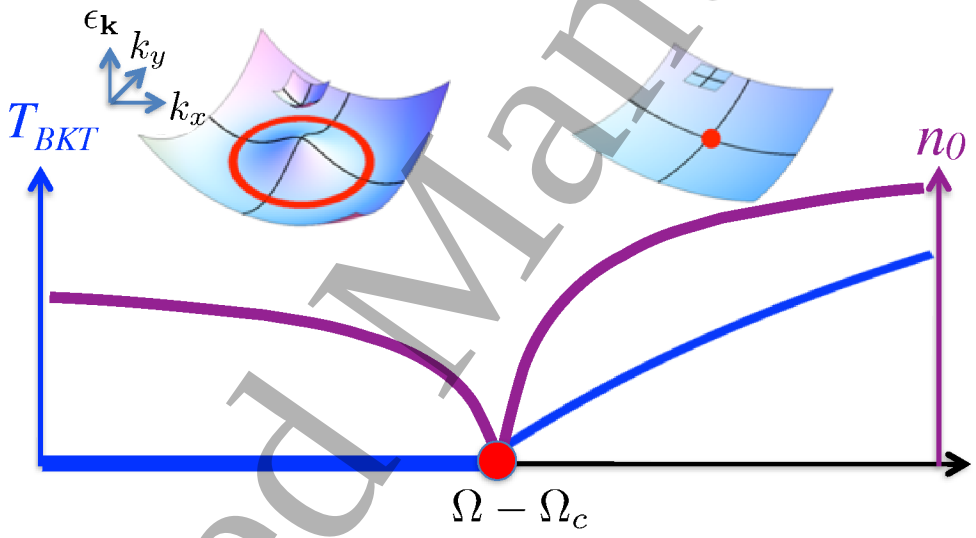

FIG. 12: Schematic of condensate fraction n_0 (purple curve) at $T = 0$ and T_{BKT} (blue curve). n_0 vanishes at the Lifshitz point, when $\Omega = \Omega_c$. It is finite on both sides of the Lifshitz point. In contrast, T_{BKT} remains zero when $\Omega < \Omega$. On this side, single-particle minimum is a circle (red circle) such that a soft mode exists in the low-energy excitations. On the other side of the Lifshitz point, single-particle minimum is unique (red dot).

Here, we consider the Hamiltonian in Eq.(18). The results can be straightforwardly generalised to 2D shaken lattices, i.e., the 2D version the Hamiltonian in Eq.(8). From Eq.(19) the resultant Density of State $\mathcal{N}(\epsilon) \sim \epsilon^{-1/2}$, we see immediately that the dimension has been effectively reduced to 1D. One concludes that condensate vanishes at the ground state. This result is identical to the case without the Zeeman energy splitting, the last term in Eq.(18). However, a key difference is that the infinite degeneracy in the single-particle spectrum disappears. Thus turning on a small interaction does not qualitatively change ground state, unlike the non-perturbative effects of interaction on the infinitely degenerate circle.

To take into account the interaction effects, we consider the ansatz

$$\Psi = e^{\frac{i\sigma_y\pi}{4}}\sqrt{\rho}e^{i\theta}\begin{pmatrix} -\sin(\phi/2)e^{-i\chi/2} \\ \cos(\phi/2)e^{i\chi/2}\end{pmatrix}, \tag{36}$$

where ρ and θ represent the density and the phase, respectively, and ϕ and χ characterize the spin orientation. The unitary transformation $U = e^{\frac{i\sigma_y\pi}{4}}$ is introduced such that there is no ambiguity in defining χ at the north or south poles of the Bloch sphere.

Using the ansatz in Eq.(36), the mean field solutions can be obtained straightforwardly to fix the values ρ_0, θ_0, χ_0, and ϕ_0. The interaction induced correction to the critical point for the quartic dispersion to emerge is given by $\Omega_c = \lambda - g_s M\rho_0/\lambda$, where $g_s = g_{12}/2 - g$ characterizes the spin-dependent part of the interaction. Thus, the critical point is not shifted if the interaction is not spin-dependent, i.e., $g_{12} = 2g$. To further obtain the effective theory to analyze the low-energy excitations, the gapped modes in the density fluctuation and the spin fluctuations can be integrated out. The low-energy excitations are dominated by the gapless phase fluctuations $\delta\theta$. For $\Omega \geq \Omega_c$, the Lagrangian is written as

$$\mathcal{L}(\theta) = \alpha_\tau(\partial_\tau\theta)^2 + \alpha(\nabla\theta)^2 + \beta(\nabla^2\theta)^2, \tag{37}$$

where $\tau = it$ is the imaginary time, $\alpha_\tau = 4(g - g_s/2)^{-1}$, $\alpha = \frac{\rho_0}{2M}(\Omega - \Omega_c)/(\lambda + \Omega - \Omega_c)$, $\beta = \frac{\rho_0}{8M}(\lambda + \Omega - \Omega_c)^{-2}$. $\delta\theta$ has been relabelled as θ to simplify notations.

Equation (37) is the so-called Quantum Lifshitz model, which is of fundamental importance in both condensed matter physics and high energy physics[95–104]. However, its realization in laboratories elude experiments so far. Synthetic SOC provides physicists a promising platform to realize and explore such fundamental model. In particular, the Lifshitz point, $\alpha = 0$ vanishes, can be reached by tuning Ω to Ω_c. At the Lifshitz point, a variety of intriguing phenomena emerge. First, the condensate fraction vanishes. This result is the same as that in non-interacting systems. Using the effective theory, the condensate fraction can be rigorously computed. Near the critical point, $n_0 \sim \delta^{\frac{1}{2K_c}}$, where $K_c = \pi(\rho_0/(2(g - g_s)M\lambda^2))^{1/2}$ and $\delta = (\Omega - \Omega_c)/\Omega_c > 0$. Second, at the critical point, the off-diagonal long-range order disappears due to the vanishing condensate fraction n_0. The one-body correlation function decays algebraically, i.e., $\langle\hat{\Psi}^\dagger_\sigma(\mathbf{r})\hat{\Psi}_\sigma(0)\rangle \sim (|\mathbf{r}|/\xi)^{-\frac{1}{2K_c}}$. Third, vortices become deconfined. In ordinary superfluids in 2D, vortices are confined at low temperatures due to the logarithmic force $U_v = 2\pi\rho_s\int d\mathbf{r}d\mathbf{r}' m(\mathbf{r})\ln|(\mathbf{r} - \mathbf{r}'|)m(\mathbf{r}')$, where $m(\mathbf{r})$ is the density of vortices at $\mathbf{r}$ and ρ_s is the superfluid stiffness [105]. Here, at the Liftshitz point, the superfluid stiffness vanishes, and the long-range Coulomb interaction among vortices disappears. The mutual interaction between vortices become a contact one, $U_v = \int d\mathbf{r}\beta(\nabla^2\theta)^2 = \beta\int d\mathbf{r}d\mathbf{r}' m(\mathbf{r})\delta^2(\mathbf{r} - \mathbf{r}')m(\mathbf{r}')$, as $\nabla^2\theta = m(\mathbf{r})$. Such contact interaction could not prevent vortices from the deconfinement. Since θ here is the phase of the bosonic field, and thus corresponds to observables that can be measured. Thus, synthetic SOC provides physicists a unique opportunity to access the deconfinement transition in the Quantum Lifshitz model. It is worth mentioning that the above analyses have assumed that the interaction is weak. A renormalization group calculation has found evidences of fermionization in the strong interacting regime, i.e., the density n scales with $\sqrt{\mu}$ [106].

The effective theory for $\Omega < \Omega_c$ has a slightly different form,

$$\mathcal{L}'(\theta) = \tilde{\alpha}_\tau(\partial_\tau\theta)^2 + \alpha_x(\partial_x\theta)^2 + \beta_x(\partial_x^2\theta)^2 + \beta_y(\partial_y^2\theta)^2 + \beta_{xy}(\partial_x\partial_y\theta)^2 + \ldots, \tag{38}$$

where all coefficients depend the microscopic parameters of the original Hamiltonian. Whereas $\mathcal{L}'(\theta)$ reduces to $\mathcal{L}(\theta)$ at the critical point, a key difference is that $\mathcal{L}'(\theta)$ still has one quartic mode along the y direction when $\Omega < \Omega_c$. This is consistent with the non-interacting systems, where the minimum of the single-particle energy forms a circle. A single quartic mode in 2D suppresses the condensate but cannot completely destroy the long-range order at the ground state in 2D. Nevertheless, it has significant effects on the Berezinsky-Kosterlitz-Thouless transition temperature $T_{\rm BKT}$. It was found out that

$$T_{\rm BKT} = \begin{cases} \sim (\Omega - \Omega_c)/\Omega_c, & \Omega \geq \Omega_c \\ 0. & \Omega < \Omega_c \end{cases}. \tag{39}$$

With decreasing Ω, $T_{\rm BKT}$ decreases down to zero at the critical point. It remains zero when $\Omega < \Omega_c$. Both the condensate fraction and T_{BKT} are shown in Fig.(12).

The results for $\Omega < \Omega_c$ also apply to a related system, in which the Hamiltonians in Eqs.(3, 14) apply to a 2D systems [46]. At a critical value of the Raman coupling strength and the shaken amplitude (or frequency), respectively, a single soft mode emerges. Thus, the condensate fraction gets suppressed, though it does not vanish.

Numerical calculations for the Hamiltonian in Eq.(3) based on variational wavefunctions have obtained consistent results [107]. The Jastrow-type wavefunction used in the numerics also indicates that the quartic dispersion leads to strong correlations. We also would like to point out that the ratio of the dimension of SOC and the dimension of the physical system is important. Though a 1D SOC in Eq.(3) or Eq.(14) does not completely change the ground state properties, their effects can be drastically enhanced in a physical 1D system. It has been shown that the Luttinger liquid parameter K can be tuned by SOC, and at the critical point where the quartic dispersion emerges, the characteristic algebraic correlations in ordinary 1D systems is replaced by exponentially decay ones[53, 108].

2. Fermions: Topological superfluids

SOC induced topological superfluids have been well studied in the literature. In particular, the interplay between SOC and strong interactions, such as that in the BEC-BCS crossover has been analyzed in a series of theoretical [109–115] and experimental [116, 117] works. Since there have been a number of review articles on interesting quantum phenomena induced by synthetic SOC in fermionic systems [118–120], including the interplay between SOC and the BEC-BCS crossover, here, we briefly mention that the Rashba coupling locks the spin on the Fermi surface such that rotating the momentum for 2π inevitably leads to a spin rotation for the same angle. In the presence of such SOC, a s-wave interaction is sufficient to create a $p_x \pm ip_y$ superfluid, i.e., a chiral topological superfluid[109, 110]. Physically, this comes from an effective p-wave interaction produced by the bare s-wave interaction in a given branch of single-particle eigenstates, which has a well defined helicity. Since this superfluid has been studied extensively, here we focus on another type of topological superfluid, $d_{x^2-y^2} \pm id_{xy}$. Such superfluid has a Chern number 2 in the bulk, and two chiral edge states in a finite system. Though it has been attracting significant interest from physicists for many years [121–124], it has not been realized in experiments yet. Here, we show that such chiral topological superfluid can be produced in a shaken lattice, which was discussed in section IV.1 [55].

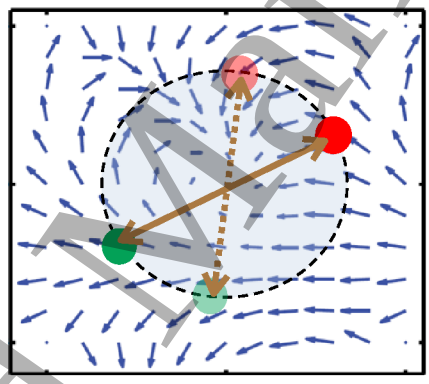

FIG. 13: (A) Effective interaction in the shaken lattice. Dashed circle represents the Fermi surface. Blue arrows represent projection of the pseudospin, which is formed by the A/B sublattices, on the $x-y$ plane. Due to the spin textures in BZ, the scattering of a hyperfine-spin-up atom (red sphere) and a hyperfine-spin-down atom (green sphere) becomes angular dependent. (B) Mean field phase diagram. n is the filling factor. Regions (I), (II) and (III) are chiral d-wave, a $s+d$-wave and a s-wave superfluid, respectively. The topological phase transition line, which separates states with Chern number 2 from those with vanishing Chern number, is highlighted using the black curve. Fig.(B) was first published in [55].

Consider two hyperfine spin states with onsite attractive interaction in a shaken checkerboard lattice,

$$U_{\text{onsite}} = -U_A \sum_{i\in A} n_{i\uparrow}n_{i\downarrow} - U_B \sum_{i\in B} n_{i\uparrow}n_{i\downarrow}. \tag{40}$$

When the interaction strengths are much weaker than the gap between the lowest two eigen bands, an effective interaction on the ground band can be obtained by projecting the U_{onsite} to this band. The BCS type of Hamiltonian is written as $U'_{\text{eff}} = -\frac{1}{N_L}\sum_{\mathbf{k}\mathbf{k}'} U_{\mathbf{k}\mathbf{k}'} d^\dagger_{\mathbf{k}\uparrow} d^\dagger_{-\mathbf{k}\downarrow} d_{-\mathbf{k}'\downarrow} d_{\mathbf{k}'\uparrow}$, where $d^\dagger_{\mathbf{k}\sigma} = \alpha_{\mathbf{k}} a^\dagger_{\mathbf{k}\sigma} + \beta_{\mathbf{k}} e^{-i\varphi_{\mathbf{k}}} b^\dagger_{\mathbf{k}\sigma}$, and N_L is the number of lattice sites. $a^\dagger_{\mathbf{k}\sigma}$ and $b^\dagger_{\mathbf{k}\sigma}$ are the corresponding operators defined in the A and B sublattices, respectively, $(\alpha_{\mathbf{k}}, \beta_{\mathbf{k}} e^{-i\varphi_{\mathbf{k}}})$ is the solution of the single-particle Hamiltonian. An interesting result is that the effective interaction $U_{\mathbf{k}\mathbf{k}'}$ depends on the angles of the scattering, as shown in Fig.(12). It can be written as

$$U_{\mathbf{k}\mathbf{k}'} = \left(U_A \alpha^2_{\mathbf{k}} \alpha^2_{\mathbf{k}'} + U_B \beta^2_{\mathbf{k}} \beta^2_{\mathbf{k}'} e^{i(\varphi_{\mathbf{k}} + \varphi_{-\mathbf{k}} - \varphi_{\mathbf{k}'} - \varphi_{-\mathbf{k}'})}\right). \tag{41}$$

This angular-dependent interaction is a lattice analogy to the Hamiltonian in Eq.(30) in the continuum. It has both the s-wave and d-wave component. This can be qualitatively understood from a novel proximity effect in the bulk between the A/B sublattices. As discussed before, the Chern band originates from the single particle tunneling between A and B sublattice, which carries a phase $e^{i\varphi_{\mathbf{k}}}$. Here, in interacting systems, the pairing tunneling of the BCS state inevitably carries phase $\sim e^{i(\varphi_{\mathbf{k}}+\varphi_{-\mathbf{k}})} \sim e^{2i\varphi_{\mathbf{k}}}$. In general, the ground state wave function can be written as

$$|G\rangle = \prod_{\mathbf{k}\in\mathbf{BZ}} (u_{\mathbf{k}} + v_{\mathbf{k}} e^{i\theta_{\mathbf{k}}} \hat{d}^{\dagger}_{\mathbf{k}\uparrow} \hat{d}^{\dagger}_{-\mathbf{k}\downarrow})|0\rangle, \tag{42}$$

where $u_{\mathbf{k}}$ and $v_{\mathbf{k}}$ are real, and $\theta_{\mathbf{k}} = \arg\{\Delta_{\mathrm{s}}\alpha^2_{\mathbf{k}} + \Delta_{\mathrm{d}}\beta^2_{\mathbf{k}} e^{i(\varphi_{\mathbf{k}}+\varphi_{-\mathbf{k}})}\}$. Δ_{s} and Δ_{d} are the order parameters for the s- and d-wave components, respectively. Thus, the ground state could be a $s + (d + id)$ superfluid. When the s-wave component is dominant, the superfluid is topologically trivial with a Chern number 1. Increasing Δ_{d} by increasing U_B/U_A or changing the single-particle Hamiltonian, there is a topological phase transition point, across which the superfluid becomes nontrivial. If one treats $d^{\dagger}_{\mathbf{k}\uparrow} d^{\dagger}_{-\mathbf{k}\downarrow}|0\rangle$ and $|0\rangle$ as the up and down component of a pseudospin $S_z = \pm 1/2$, we see that the Chern number becomes 2 when Δ_{d} is dominant. Consequently, two chiral edge states emerge in a finite system with sharp edges. The chiral d-wave superfluid of atoms can be detected by a variety of techniques, ranging the expansion of the atomic cloud to angular-momentum-sensitive Bragg spectroscopy [125–129].

It is useful to compare the underlying mechanisms for the chiral p- and d-wave superfluids induced by SOC. In the p-wave superfluid, hyperfine spin states are coupled to each other in the single-particle Hamiltonian. In contrast, different orbitals in a lattice are used for the d-wave superfluid. In non-interacting systems, both the hyperfine spin states and the orbitals can be defined as a pseudospin, and the resultant single-particle Hamiltonians are equivalent. However, in interacting systems, it is the different microscopic degrees of freedom that give rise to distinct effective interactions and superfluids. In p-wave superfluids, "spin"-up and "spin"-down particles interact with the s-wave scatterings. In the d-wave case, "spin"-up and "spin"-down particles do not interact. One need to include two different hyperfine spin states, which are governed by the same single-particle Hamiltonian in Eq.(21) and meanwhile interact with each other through Eq.(40). The interplay between the hyperfine spin and the pseudospin, which represents the orbital degree of freedom in a lattice, produces the chiral d-wave superfluid. This comparison is an illuminating example that the highly controllable atomic systems indeed provides physics an ideal playground to explore very rich quantum states and quantum phenomena that may not easy to access in other systems.

Besides attractive interactions, repulsive interactions have also been studied in Chern bands. Both analytical and numerical methods have been used to explore a variety of magnetic orderings [130–132]. An important question as to whether the non-trivial topological characters and antiferromagnetic long-range order could coexist is worth more studies [133].

VI. Challenges and outlook

Whereas a lot of important progresses in exploring synthetic gauge fields have been made in the past a few years, there also exist challenges in current studies. Most experiments have been working on alkali atoms so far. When applying the Raman lasers to such atoms, the spontaneous emission induces the heating of the quantum gas. In particular, the fine splitting in the atomic structure of alkali atoms leads to a heating of the same order of the Raman coupling strength [29]. This is one of the main obstacles for realizing interacting topological matters of fermionic atoms. Though the issue of fine structure splitting is not relevant to shaken lattices, heating effects exist when atoms experience a lattice potential that is moving back and forth in the real space [134, 135]. The Floquet driven heats the quantum gas because of the excitation produced by interactions in eigenstates of the driven system. In particular, when the interaction could scatter resonantly two particles from one band to two other bands, the heating may become severe [136]. So far, most experimental studies have been focusing on band structures of non-interacting systems.

To overcome the heating problem, atomic species that do not suffer the fine structure splitting could be used. The ultra-narrow optical clock transition between two electronic orbital states of ^{87}Sr significantly reduces the heating rate. This atomic clock lattice scheme provides physicists a promising platform to explore interacting topological matters at low temperatures [20, 21]. In optical lattices, band structures could be engineered such that certain sources for the heating, such as the decay due to two-body scatterings, may be suppressed [137, 138]. In a current experiment on optical lattice, interaction effects on the dynamics of bosons in a Harper-Hofstadter model have been investigated [139]. The orbital degree of freedom that was recently used allow experimentalists to control the inter- and intra-psuedospin interaction such that a stripe phase of BEC is directly observed [40]. All these exciting recent developments show that, after years of studies of synthetic gauge fields, a new era awaits physics to explore many new quantum phenomena that will be brought by synthetic gauge fields and its interplay with the highly tunable atoms.

[1] J. Dalibard, F. Gerbier, G. Juzelinas, and P. Öhberg, *Artificial gauge potentials for neutral atoms*, Rev. Mod. Phys. **83**, 1523 (2011).
[2] Y.-J. Lin, K. K. Jimenez-Garcia, and I. B. Spielman, *Spin-orbit-coupled Bose-Einstein condensates*, Nature, **471**, 83 (2011).
[3] Y.-J. Lin, R. L. Compton, A. R. Perry, W.D. Phillips, J. V. Porto, and I. B. Spielman, *Bose-Einstein condensate in a uniform light-induced vector potential*, Phys. Rev. Lett. **102**, 130401 (2009).
[4] Y.-J. Lin, R. L. Compton, K. Jimenez-Garcia, J. V. Porto , and I. B. Spielman, *Synthetic magnetic fields for ultracold neutral atoms*, Nature, **462**, 628 (2009).
[5] Y-J. Lin, R. L. Compton, K. Jimenez-Garcia, W. D. Phillips, J. V. Porto, and I. B. Spielman, *A synthetic electric force acting on neutral atoms*, Nature Physics, **7**, 531 (2011).
[6] P. Wang, Z.-Q. Yu, Z. Fu, J. Miao, L. Huang, S. Chai, H. Zhai, and J. Zhang, *Spin-Orbit Coupled Degenerate Fermi Gases*, Phys. Rev. Lett. **109**, 095301 (2012).
[7] L. W. Cheuk, A. T. Sommer, Z. Hadzibabic, T. Yefsah, W. S. Bakr, and M. W. Zwierlein, *Spin-Injection Spectroscopy of a Spin-Orbit Coupled Fermi Gas*, Phys. Rev. Lett. **109**, 095302 (2012).
[8] J.-Y. Zhang, S.-C. Ji, Z. Chen, L. Zhang, Z.-D. Du, B. Yan, G.-S. Pan, B. Zhao, Y.-J. Deng, H. Zhai, S. Chen, and J.-W. Pan, *Collective Dipole Oscillations of a Spin-Orbit Coupled Bose-Einstein Condensate*, Phys. Rev. Lett. **109**, 115301 (2012).
[9] C. Qu, C. Hamner, M. Gong, C. Zhang, and P. Engels, *Observation of Zitterbewegung in a spin-orbit-coupled Bose-Einstein condensate*, Phys. Rev. A, **88**, 021604(R) (2013).
[10] A. J. Olson, S.-J. Wang, R. J. Niffenegger, C.-H. Li, C. H. Greene, and Y. P. Chen, *Tunable Landau-Zener transitions in a spin-orbit-coupled Bose-Einstein condensate*, Phys. Rev. A, **90**, 013616 (2014).
[11] M. Aidelsburger, M. Atala, M. Lohse, J. T. Barreiro, B. Paredes, and I. Bloch, *Realization of the Hofstadter Hamiltonian with Ultracold Atoms in Optical Lattices*, Phys. Rev. Lett. **111**, 185301 (2013).
[12] H. Miyake, G. A. Siviloglou, C. J. Kennedy, W. C. Burton, and W. Ketterle, *Realizing the Harper Hamiltonian with Laser-Assisted Tunneling in Optical Lattices*, Phys. Rev. Lett. **111**, 185302 (2013).
[13] G. Jotzu, M. Messer, R. Desbuquois, M. Lebrat, T. Uehlinger, D. Greif, and T. Esslinger, *Experimental realization of the topological Haldane model with ultracold fermions*, Nature, **515**, 237 (2014).
[14] C. V. Parker, L.-C. Ha, and C. Chin, *Direct observation of effective ferromagnetic domains of cold atoms in a shaken optical lattice*, Nature Physics, **9**, 769 (2013).
[15] J. Struck, M. Weinberg, C. Ölschläger, P. Windpassinger, J. Simonet, K. Sengstock, R. Höppner, P. Hauke, A. Eckardt, M. Lewenstein, and L. Mathey, *Engineering Ising-XY spin-models in a triangular lattice using tunable artificial gauge fields*, Nature Physics, **9**, 738 (2013).
[16] B. K. Stuhl, H.-I. Lu, L. M. Aycock, D. Genkina, and I. B. Spielman, *Visualizing edge states with an atomic Bose gas in the quantum Hall regime*, Science, **349**, 1514 (2015).
[17] M. Mancini, G. Pagano, G. Cappellini, L. Livi, M. Rider, J. Catani, C. Sias, P. Zoller, M. Inguscio, M. Dalmonte, and L. Fallani, *Observation of chiral edge states with neutral fermions in synthetic Hall ribbons*, Science, **349**, 1510 (2015).
[18] N. Q. Burdick, Y. Tang, and B. L. Lev, *Long-Lived Spin-Orbit-Coupled Degenerate Dipolar Fermi Gas* Phys. Rev. X, **6**, 031022 (2016).
[19] B. Song, C. He, S. Zhang, E. Hajiyev, W. Huang, X.-J. Liu, and G.-B. Jo, *Spin-orbit-coupled two-electron Fermi gases of ytterbium atoms*, Phys. Rev. A, **94**, 061604(R) (2016).
[20] S. Kolkowitz, S. L. Bromley, T. Bothwell, M. L. Wall, G. E. Marti, A. P. Koller, X. Zhang, A. M. Rey, and J. Ye, *Spin-orbit-coupled fermions in an optical lattice clock*, Nature **542**, 66-70 (2017)
[21] L. F. Livi, G. Cappellini, M. Diem, L. Franchi, C. Clivati, M. Frittelli, F. Levi, D. Calonico, J. Catani, M. Inguscio, and L. Fallani, *Synthetic Dimensions and Spin-Orbit Coupling with an Optical Clock Transition*, Phys. Rev. Lett. **117**, 220401 (2016).
[22] L. Huang, Z. Meng, P. Wang, P. Peng, S. L. Zhang, L. Chen, D. Li, Q. Zhou, and J. Zhang, *Experimental realization of two-dimensional synthetic spin-orbit coupling in ultracold Fermi gases*, Nature Physics, **12**, 540 (2016).
[23] Z. Wu, L. Zhang, W. Sun, X.-T. Xu, B.-Z. Wang, S.-C. Ji, Y. Deng, S. Chen, X.-J. Liu, and J.-W. Pan, *Realization of Two-Dimensional Spin-orbit Coupling for Bose-Einstein Condensates*, Science **354**, 83-88 (2016)
[24] E. J. Meier, F. A. An, B. Gadway, *Observation of the topological soliton state in the Su-Schrieffer-Heeger model*, Nature Communications, **7**, 13986 (2016).
[25] F. A. An, E. J. Meier, B. Gadway, *Flux-dependent localisation in a disordered flat-band lattice*, arXiv:1705.09268, preprint
[26] H. Zhai, *Spin-orbit coupled quantum gases*, Int. J. Mod. Phys. B. **26**, 1230001 (2012).
[27] Victor Galitski, Ian B. Spielman, *Spin-orbit coupling in quantum gases*, Nature **494**, 49-54 (2013).
[28] N. Goldman, G. Juzeliunas, P. Ohberg, I. B. Spielman, *Light-induced gauge fields for ultracold atoms*, Rep. Prog. Phys. **77** 126401 (2014).
[29] H. Zhai, *Degenerate Quantum Gases with Spin-Orbit Coupling*, Rep. Prog. Phys.**78**, 026001 (2015)
[30] T.-L. Ho, S. Z. Zhang, *Bose-Einstein condensates with spin-orbit interaction*, Phys. Rev. Lett. **107**, 150403 (2011).
[31] D. L. Campbell, G. Juzeliunas, and I. Spielman, *Realistic Rashba and Dresselhaus spin-orbit coupling for neutral atoms*, Phys. Rev. A **84**, 025602 (2011).
[32] R. G. Unanyan, B. W. Shore, and K. Bergmann, *Laser-driven population transfer in four-level atoms: consequences of*

non-Abelian geometrical adiabatic phase factors, Phys. Rev. A **59**, 2910?2919 (1999).
[33] J. Ruseckas, G, Juzeliunas, P. hberg, and M. Fleischhauer, *Non-Abelian gauge potentials for ultracold atoms with degenerate dark states*, Phys. Rev. Lett. **95**, 010404 (2005).
[34] T. D. Stanescu, C. Zhang, and V. Galitski, *Nonequilibrium spin dynamics in a trapped Fermi gas with effective spin-orbit interactions*, Phys. Rev. Lett. **99**,110403 (2007).
[35] D. Jaksch and P. Zoller, *Creation of effective magnetic fields in optical lattices: the Hofstadter butterfly for cold neutral atoms*. New J. Phys. **5**, 56 (2003).
[36] F. Gerbier and J. Dalibard, *Gauge fields for ultracold atoms in optical superlattices*, New J. Phys. **12**, 033007 (2010).
[37] E. J. Mueller, *Artificial electromagnetism for neutral atoms: Escher staircase and Laughlin liquids*, Phys. Rev. A 70, 041603 (2004).
[38] M. Aidelsburger, M. Atala, S. Nascimbène, S. Trotzky, Y.-A. Chen, and I. Bloch, *Experimental Realization of Strong Effective Magnetic Fields in an Optical Lattice*, Phys. Rev. Lett. **107**, 255301 (2011).
[39] J. Li, W. Huang, B. Shteynas, S. Burchesky, F. C. Top, E. Su, J. Lee, A. O. Jamison, W. Ketterle, *Spin-Orbit Coupling and Spin Textures in Optical Superlattices*, Phys. Rev. Lett. 117, 185301 (2016)
[40] J. Li, J. Lee, W. Huang, S. Burchesky, B.Shteynas, F. C.Top, A. O. Jamison, W. Ketterle, *Observation of the supersolid stripe phase in spin-orbit coupled Bose-Einstein condensates*, Nature **543**, 91-94 (2017).
[41] Yun Li, Lev P. Pitaevskii, Sandro Stringari, *Quantum tri-criticality and phase transitions in spin-orbit coupled Bose-Einstein condensates*, Phys. Rev. Lett. 108, 225301 (2012)
[42] C. Wang, C. Gao, C. M. Jian, and H. Zhai, *Spin-orbit coupled spinor Bose-Einstein condensates*, Phys. Rev. Lett. **105**, 160403 (2010).
[43] H. Lignier, C. Sias, D. Ciampini, Y. Singh, A. Zenesini, O. Morsch, and E. Arimondo, *Dynamical Control of Matter-Wave Tunneling in Periodic Potentials*, Phys. Rev. Lett. **99**, 220403 (2007).
[44] W. Zheng, and H. Zhai, *Floquet Topological States in Shaking Optical Lattices*, Phys. Rev. A 89, 061603 (2014)
[45] S. L. Zhang, and Q. Zhou, *Shaping topological properties of the band structures in a shaken optical lattice*, Phys. Rev. A **90**, 051601(R) (2014)
[46] H. C. Po, and Q. Zhou, *A two-dimensional algebraic quantum liquid produced by an atomic simulator of the quantum Lifshitz model*, Nat. Comm. **6**, 8012 (2015).
[47] J. Miao, B. Liu, and W. Zheng, *Quantum Phase Transition of Bosons in a Shaken Optical Lattice*, Phys. Rev. A 91, 033404 (2015)
[48] J. P. Vyasanakere, and V. B. Shenoy, *Bound states of two spin-1/2 fermions in a synthetic non-Abelian gauge field*, Phys. Rev. B, **83**, 094515 (2011).
[49] X. L. Cui, and Q. Zhou, *Enhancement of condensate depletion due to spin-orbit coupling*, Phys. Rev. A, **87**, 031604(R) (2013).
[50] Q. Zhou, and X. L. Cui, *Fate of a Bose-Einstein Condensate in the Presence of Spin-Orbit Coupling*, Phys. Rev. Lett. **110**, 140407 (2013).
[51] N. D. Mermin and H. Wagner, *Absence of Ferromagnetism or Antiferromagnetism in One- or Two-Dimensional Isotropic Heisenberg Models*, Phys. Rev. Lett. **17**, 1133 (1966).
[52] W. Zheng, Z.-Q. Yu, X. Cui, and H. Zhai, *Properties of Bose Gases with Raman-Induced Spin-Orbit Coupling*, J. Phys. B, 46, 134007 (2013)
[53] H. C. Po, W. Chen, and Q. Zhou, *Non-Luttinger quantum liquid of one-dimensional spin-orbit-coupled bosons*, Phys. Rev. A 90, 011602(R) (2014)
[54] J. Zak, *Berry's phase for energy bands in solids*, Phys. Rev. Lett. 62, 2747 (1989)
[55] S. L. Zhang, L. J. Lang, and Q. Zhou, *Chiral d-wave superfluid in periodically driven lattices*, Phys. Rev. Lett. **115**, 225301 (2015).
[56] A. Eckardt, C. Weiss, and M. Holthaus, *Superfluid-Insulator Transition in a Periodically Driven Optical Lattice*, Phys. Rev. Lett. **95**, 260404 (2005).
[57] M. Greiner, O. Mandel, T. Esslinger, T. W. Hänsch, and I. Bloch, *Quantum phase transition from a superfluid to a Mott insulator in a gas of ultracold atoms*, Nature, **415**, 39 (2002).
[58] L. Tarruell, D. Greif, T. Uehlinger, G. Jotzu, and T. Esslinger, *Creating, moving and merging Dirac points with a Fermi gas in a tunable honeycomb lattice*, Nature, **483**, 302 (2012).
[59] M. Atala, M. Aidelsburger, J. T. Barreiro, D. Abanin, T. Kitagawa, E. Demler, and I. Bloch, *Direct measurement of the Zak phase in topological Bloch bands*, Nature Physics, **9**, 795 (2013).
[60] T. Li, L. Duca, M. Reitter, F. Grusdt, E. Demler, M.Endres, M. Schleier-Smith, I. Bloch, and U. Schneider, *Bloch state tomography using Wilson lines*, Science **352**, 1094 (2016)
[61] F. Wilczek, and A. Zee,*Appearance of Gauge Structure in Simple Dynamical Systems*, Phys. Rev. Lett. **52**, 2111 (1984).
[62] Q. Z. Wang, and C. X. Liu, *Topological nonsymmorphic crystalline superconductors*, Phys. Rev. B **93**, 020505(R) (2016).
[63] C. Fang, and L. Fu, *New classes of three-dimensional topological crystalline insulators: Nonsymmorphic and magnetic*, Phys. Rev. B **91**, 161105(R) (2015).
[64] K. Shiozaki, M. Sato, and K. Gomi, *Z_2 topology in nonsymmorphic crystalline insulators: Mbius twist in surface states*, Phys. Rev. B **91**, 155120 (2015).
[65] S.-L. Zhang, and Q. Zhou, *A two-leg Su-Schrieffer-Heeger chain with glide reflection symmetry*, Phys. Rev. A, **95**, 061601 (2017).
[66] X.-J. Liu, Z.-X. Liu, and M. Cheng, *Manipulating Topological Edge Spins in a One-Dimensional Optical Lattice*, Phys. Rev. Lett. **110**, 076401 (2013).

[67] L.-J. Lang, S.-L. Zhang, and Q. Zhou, *Nodal Brillouin Zone Boundary from Folding a Chern Insulator*, Phys. Rev. A, **95**, 053615 (2017).
[68] A. Celi, P. Massignan, J. Ruseckas, N. Goldman, I.B. Spielman, G. Juzeliunas, and M. Lewenstein, *Synthetic Gauge Fields in Synthetic Dimensions*, Phys. Rev. Lett. **112**, 043001 (2014)
[69] M. Mancini, G. Pagano, G. Cappellini, L. Livi, M. Rider, J. Catani, C. Sias, P. Zoller, M. Inguscio, M. Dalmonte, and L. Fallani, *Observation of chiral edge states with neutral fermions in synthetic Hall ribbons*, Science, **349**, 510-1513, (2015)
[70] B. K. Stuhl, H.-I Lu, L. M. Aycock, D. Genkina, and I. B. Spielman, *Visualizing edge states with an atomic Bose gas in the quantum Hall regime*, Science **349**, 1514-1518 (2015)
[71] O. Boada, A. Celi, J. Rodríguez-Laguna, J. I. Latorre, and M. Lewenstein, *Quantum simulation of non-trivial topology*, New Journal of Physics **17**, 045007 (2015)
[72] P. Nozières, in *Bose-Einstein Condensation*, edited by A. Griffin, D. W. Snoke, and S. Stringari, Cambridge University Press, Cambridge, (1995)
[73] E. J. Mueller, T.L. Ho, M. Ueda, and G. Baym, *Fragmentation of Bose-Einstein Condensates*, Phys. Rev. A **74**, 033612 (2006)
[74] C. K. Law, H. Pu, and N. P. Bigelow, *Quantum Spins Mixing in Spinor Bose-Einstein Condensates*, Phys. Rev. Lett. **81**, 5257 (1998).
[75] T.-L. Ho, and S. K. Yip, *Fragmented and Single Condensate Ground States of Spin-1 Bose Gas*, Phys. Rev. Lett. **84**, 4031 (2000)
[76] C. Wu, I. Mondragon-Shem and X.-F. Zhou, *Unconventional Bose Einstein condensations from spin-orbit coupling*, Chin. Phys. Lett. **28**, 097102 (2011).
[77] T. Stanescu, B. Anderson, and V. Galitski, *Spin-orbit coupled Bose-Einstein condensates*, Phys. Rev. A **78**, 023616 (2008)
[78] S.-C. Ji, J.-Y. Zhang, L. Zhang, Z.-D. Du, W. Zheng, Y.-J. Deng, H. Zhai, S. Chen, and J.-W. Pan, *Experimental Determination of the Finite-Temperature Phase Diagram of a Spin-Orbit Coupled Bose Gas*, Nature Physics **10**, 314 (2014)
[79] Z.-Q. Yu, *Equation of state and phase transition in spin-orbit-coupled Bose gases at finite temperature: A perturbation approach*, Phys. Rev. A 90, 053608 (2014)
[80] J. Radic, S. S. Natu, and V. Galitski, *Stoner ferromagnetism in a thermal pseudospin-1/2 Bose gas*, Phys. Rev. Lett. **113**, 185302 (2014)
[81] C. Hickey, and A. Paramekanti, *Thermal Phase Transitions of Strongly Correlated Bosons with Spin-Orbit Coupling*, Phys. Rev. Lett. **113**, 265302 (2014)
[82] R. A. Williams, L. J. LeBlanc, K. Jimenez-Garcia, M. C. Beeler, A. R. Perry, W. D. Phillips, I. B. Spielman, *Synthetic partial waves in ultracold atomic collisions*, Science **335**, 314-317 (2012)
[83] S, Gopalakrishnan, A. Lamacraft, and P. M. Goldbart, *Universal phase structure of dilute Bose gases with Rashba spin-orbit coupling*, Phys. Rev. A 84, 061604(R) (2011)
[84] T. Ozawa, and G. Baym, *Renormalization of interactions of ultracold atoms in simulated Rashba gauge fields*, Phys. Rev. A **84**, 043622 (2011)
[85] Z. Xu, Z. Yu, and S. Zhang, *Evidence for correlated states in a cluster of bosons with Rashba spin-orbit coupling*, New J. Phys. **18** 025002 (2016)
[86] T. A. Sedrakyan, A. Kamenev, and L. I. Glazman, *Composite fermion state of spin-orbit coupled bosons*, Phys. Rev. A **86**, 063639 (2012)
[87] T. A. Sedrakyan, L. I. Glazman, and A. Kamenev, *Absence of Bose condensation on lattices with moat bands*, Phys. Rev. B **89**, 201112(R) (2014)
[88] T. A. Sedrakyan, L. I. Glazman, and A. Kamenev, *Spontaneous formation of a non-uniform chiral spin liquid in moat-band lattices*, Phys. Rev. Lett. **114**, 037203 (2015)
[89] S. Sinha, R. Nath, and L. Santos, *Trapped two-dimensional condensates with synthetic spin-orbit coupling*, Phys. Rev. Lett. **107**, 270401 (2011)
[90] X. Zhou, J. Zhou, and C. Wu, *Vortex structures of rotating spin-orbit coupled Bose-Einstein condensates*, Phys. Rev. A **84**, 063624 (2011)
[91] B. Ramachandhran, Bogdan Opanchuk, Xia-Ji Liu, Han Pu, Peter D. Drummond, Hui Hu, *Half-quantum vortex state in a spin-orbit coupled Bose-Einstein condensate*, Physical Review A **85**, 023606 (2012)
[92] R. Barnett, S. Powell, T. Graß, M. Lewenstein and S. Das Sarma, Phys. Rev. A **85**, 023615 (2012).
[93] T. Ozawa, and G. Baym *Stability of ultracold atomic Bose condensates with Rashba spin-orbit coupling against quantum and thermal fluctuations*, Phys. Rev. Lett. **109**, 025301 (2012)
[94] T. Ozawa and G. Baym, *Ground-state phases of ultracold bosons with Rashba-Dresselhaus spin-orbit coupling*, Phys. Rev. A **85**, 013612 (2012).
[95] Fradkin, E., *Field Theories of Condensed Matter Physics*, (Addison Wesley, Redwood City, 2nd Edition, (2013)
[96] Rokhsar, D. S. and Kivelson, S. A. *Superconductivity and the quantum hard-core dimer gas.* Phys. Rev. Lett. **61**, 2376 (1988)
[97] Moessner R and Raman K S, *Quantum dimer models*, *Introduction to Frustrated Magnetism*, Chapter 17 (Springer Berlin Heidelberg, 2011)
[98] R. Moessner and S. L. Sondhi, *Resonating Valence Bond Phase in the Triangular Lattice Quantum Dimer Model*, Phys. Rev. Lett. **86**, 1881 (2001)
[99] B. Hsu, and E. Fradkin, *Dynamical stability of the quantum Lifshitz theory in 2+1 Dimensions*, Phys. Rev. B **87**, 085102 (2013)

[100] A. Vishwanath, L. Balents, and T. Senthil, *Quantum Criticality and Deconfinement in PhaseTransitions Between Valence Bond Solids*, Phys. Rev. B **69**, 224416 (2004)
[101] Hořava, P., *Membranes at Quantum Criticality*, J. High Energy Phys. 0903, 020 (2009)
[102] Hořava, P., *Quantum gravity at a Lifshitz point*, Phys. Rev. D **79**, 084008 (2009)
[103] M. Baggio, J. de Boer, and K. Holsheimer, *Anomalous Breaking of Anisotropic Scaling Symmetry in the Quantum Lifshitz Model*, Journal of High Energy Physics 2012:99 (2012)
[104] Charmousis, C., Niz, G., Padilla, A., and Saffin, P., *Strong coupling in Horava gravity*, Journal of High Energy Physics (08): 070 (2009).
[105] Kosterlitz, J. M. and Thouless, D. J., Ordering, *metastability and phase transitions two-dimensional systems*, J. Phys. C: Solid State Phys. **6**, 1181-1203 (1973)
[106] J. Wu, and C. Wu, *Quantum Criticality of the Two-dimensional Bose Gas with the Lifshitz dispersion*, arXiv:1509.03953, preprint.
[107] J. Radic, S. S. Natu, and V. Galitski, *Strong correlation effects in a two-dimensional Bose gas with quartic dispersion*, Phys. Rev. A **91**, 063634 (2015)
[108] S. Uchino and A. Tokuno, *Population-imbalance instability in a Bose-Hubbard ladder in the presence of a magnetic flux*, Phys. Rev. A **92**, 013625 (2015)
[109] C. Zhang, S. Tewari, R. M. Lutchyn, and S. D. Sarma, $p_x + ip_y$ *superfluid from s-wave interactions of fermionic cold atoms*, Phys. Rev. Lett. **101**, 160401 (2008).
[110] M. Sato, Y. Takahashi, and S. Fujimoto, *Non-Abelian topological order in s-wave superfluids of ultracold fermionic atoms*, Phys. Rev. Lett. **103**, 020401 (2009).
[111] J. P. Vyasanakere, S. Zhang, and V. B. Shenoy, *BCS-BEC crossover induced by a synthetic non-Abelian gauge field*, Phys. Rev. B **84**, 014512 (2011).
[112] M. Gong, S. Tewari, and C. Zhang, *BCS-BEC Crossover and Topological Phase Transition in 3D Spin-Orbit Coupled Degenerate Fermi Gases*, Phys. Rev. Lett. **107**, 195303 (2011).
[113] H. Hu, L. Jiang, X.-J. Liu, and H. Pu, *Probing Anisotropic Superfluidity in Atomic Fermi Gases with Rashba Spin-Orbit Coupling*, Phys. Rev. Lett. **107**, 195304 (2011).
[114] Z.-Q. Yu and H. Zhai, *Spin-Orbit Coupled Fermi Gases across a Feshbach Resonance*, Phys. Rev. Lett. **107**, 195305 (2011).
[115] J. P. A. Devreese, J. Tempere, and C. A. R. Sá de Melo, *Effects of Spin-Orbit Coupling on the Berezinskii-Kosterlitz-Thouless Transition and the Vortex-Antivortex Structure in Two-Dimensional Fermi Gases*, Phys. Rev. Lett. **113**, 165304 (2014).
[116] R. A. Williams, M. C. Beeler, L. J. LeBlanc, K. Jiménez-García, and I. B. Spielman, *Raman-Induced Interactions in a Single-Component Fermi Gas Near an s-Wave Feshbach Resonance*, Phys. Rev. Lett. 111, 095301 (2013).
[117] L. Huang, P. Wang, P. Peng, Z. Meng, L. Chen, P. Zhang, J. Zhang, *Dissociation of Feshbach molecules via spin-orbit coupling in ultracold Fermi gases*, Phys. Rev. A 91, 041604(R) (2015)
[118] J. Zhang, H. Hu, X.-J. Liu, H. Pu, *Fermi Gases with Synthetic Spin-Orbit Coupling*, Annu. Rev. Cold At. Mol. 2, 81 (2014)
[119] H. Zhai, *Degenerate quantum gases with spin-orbit coupling: a review*, Rep. Prog. Phys. **78**, 026001 (2015).
[120] W. Yi, W. Zhang, and X. Cui, *Pairing Superfluidity in Spin-Orbit Coupled Ultracold Fermi Gases*, Sci. China: Phys. Mech. Astron. 58, 014201 (2015).
[121] N. Read and D. Green, Phys. Rev. B, *Paired states of fermions in two dimensions with breaking of parity and time-reversal symmetries and the fractional quantum Hall effect*, **61**, 10267 (2000).
[122] G. E. Volovik, *On edge states in superconductors with time inversion symmetry breaking*, JETP Lett. **66**, 522 (1997).
[123] R. B. Laughlin, *Magnetic Induction of* $d_{x2-y2}+id_{xy}$ *Order in High-Tc Superconductors*, Phys. Rev. Lett. **80**, 5188 (1998).
[124] R. Nandkishore, L. S. Levitov, and A. V. Chubukov, *Chiral superconductivity from repulsive interactions in doped graphene*, Nature Physics **8**, 158-163 (2012)
[125] X.-J. Liu, X. Liu, C. Wu, and J. Sinova, *Quantum anomalous Hall effect with cold atoms trapped in a square lattice*, Phys. Rev. A **81**, 033622 (2010).
[126] I. B. Spielman, *Detection of topological matter with quantum gases*, Ann. Phys. (Berlin) **525**, 797 (2013).
[127] N. Goldman, J. Dalibard, A. Dauphin, F. Gerbier, M. Lewenstein, P. Zoller, and I. B. Spielman, *Direct imaging of topological edge states in cold-atom systems*, Proc. Natl. Acad. Sci. U.S.A. **110**, 6736 (2013).
[128] N. Goldman, J. Beugnon, and F. Gerbier, *Detecting chiral edge states in the Hofstadter optical lattice*, Phys. Rev. Lett. **108**, 255303 (2012).
[129] V. Galitski, and I. B. Spielman, *Spin-orbit coupling in quantum gases*, Nature, **494**, 49 (2013).
[130] W. Zheng, H. Shen, Z. Wang, and H. Zhai, *Magnetic Order Driven Topological Transition in the Haldane-Hubbard Model*, Phys. Rev. B **91**, 161107(R) (2015)
[131] C. Hickey, L. Cincio, Z. Papić, and A. Paramekanti, *Haldane-Hubbard Mott Insulator: From Tetrahedral Spin Crystal to Chiral Spin Liquid*, Phys. Rev. Lett. **116**, 137202 (2016)
[132] T. I. Vanhala, T. Siro, L. Liang, M. Troyer, A. Harju, and P. Törmä, *Topological phase transitions in the repulsively interacting Haldane-Hubbard model*, Phys. Rev. Lett. **116**, 225305 (2016)
[133] J. Imriška, L. Wang, and M. Troyer, *First order topological phase transition of the Haldane–Hubbard model*, Phys. Rev. B **94**, 035109 (2016)
[134] E. Anisimovas, G. Žlabys, B. M. Anderson, G. Juzeliūnas, and A. Eckardt, *Role of real-space micromotion for bosonic and fermionic Floquet fractional Chern insulators*, Phys. Rev. B **91**, 245135 (2015).

[135] M. Račiūnas, G. Žlabys, A. Eckardt, and E. Anisimovas, *Modified interactions in a Floquet topological system on a square lattice and their impact on a bosonic fractional Chern insulator state*, Phys. Rev. A **93**, 043618 (2016).
[136] S. Choudhury and E. J. Mueller, *Stability of a Bose-Einstein condensate in a driven optical lattice: Crossover between weak and tight transverse confinement*, Phys. Rev. A, 91, 063639 (2015).
[137] S. Choudhury and E. J. Mueller, *Transverse collisional instabilities of a Bose-Einstein condensate in a driven one-dimensional lattice*, Phys. Rev. A 91, 023624 (2015).
[138] S. Choudhury and E. J. Mueller, *Stability of a Floquet Bose-Einstein condensate in a one-dimensional optical lattice*, Phys. Rev. A 90, 0136121 (2014).
[139] M. E. Tai, A. Lukin, M. Rispoli, R.Schittko, T. Menke, D. Borgnia, P. M. Preiss, F. Grusdt, A. M. Kaufman, and M. Greiner, *Microscopy of the interacting Harper-Hofstadter model in the few-body limit*, arXiv:1612.05631, preprint.